

Intrapulse Radar-Embedded Communications via Multi-objective Optimization

D. Ciuonzo, A. De Maio, G. Foglia, M. Piezzo

Abstract—We deal with the problem of intrapulse radar-embedded communication, and propose a novel waveform design procedure based on a multi-objective optimization paradigm. More specifically, under both energy and similarity constraints, we devise signals according to the following criterion: constrained maximization of the Signal-to-Interference Ratio (SIR) and constrained minimization of a suitable correlation index (which is related to the possibility of waveform interception). This is tantamount to jointly maximizing two competing quadratic forms under two quadratic constraints, so that the problem can be formulated in terms of a non-convex multi-objective optimization. In order to solve it, we resort to the scalarization technique, which reduces the vectorial problem into a scalar one using Pareto weights defining the relative importance of the two objectives. At the analysis stage, we assess the performance of the proposed waveform design scheme in terms of Symbol Error Rate (SER) and the so-called “intercept metric”.

Index Terms—Communication symbol design, Low-Probability of Intercept (LPI) communications, Radar-embedded communications, Multi-objective optimization problem, Pareto-optimal points, Radio Frequency IDentification (RFID).

I. INTRODUCTION

THE CAPABILITY of establishing a covert communication has always represented a critical issue for defense-related applications, where one among the key aspects is the possibility to hide sensitive information to hostile interceptors. Along the years, various strategies have been proposed as viable means of masking the data transmission; excellent discussions on the topic can be found in [2], [3].

An interesting option consists in directly exploiting a waveform which is already present in the probed environment, such as pre-existing communication transmissions [4] or the actual radar backscattered interference [5], [6], [7]. In this case, a radio frequency tag/transponder, such as a Radio Frequency Identifier (RFID) [8], is first employed to suitably remodulate the incident radiation, then to embed the devised communication signal in the ambient electromagnetic background, thus providing a natural masking in dense and cluttered environment. The research production for this class of approaches has

been quite fertile; in fact, starting from the seminal work of [9] (who introduced the idea of using modulated reflectors for communication), various tag-based Radar-EMbedded (REM) modulation techniques have been proposed. We may cite, for instance, [5], [10], and [11], where the radar illumination is modulated on an inter-pulse basis applying phase-shift sequences over known Coherent Processing Intervals (CPI). However, even though a Low Probability of Intercept (LPI) is ensured (since the signaling is covert by the radar backscatter), a low data-rate is provided (in the order of bits-per-CPI). Such data rate can be acceptable only in very special cases [2] but, unfortunately, in general the aforementioned rate is too low to establish an acceptable communication link. More recently, in [12] an overview discussion on possibilities and challenges for co-existence of radar operations and communication systems was provided. Additionally, a theoretical study on achievable information bounds for radar and communication systems co-existence appeared in [13].

In [2], the authors propose a novel intrapulse REM communication procedure based on the remodulation of the incident radar signaling, through an RF tag/transponder (within the probed environment), into one of the possible K different communication waveforms (acting as information symbols). Three approaches to the waveform design problem have been presented and thoughtfully investigated. The idea is to properly exploit the natural masking provided by the ambient scatter, by devising symbols sharing a certain correlation with the surrounding radar reflections, so as to make very hard the recovery of the information for a hostile eavesdropper (thus ensuring a LPI). Moreover, the transmit sequences are sufficiently separated (ideally orthogonal) with one another in order to minimize the mutual interference, thus ensuring a low Symbol Error Rate (SER) or Bit Error Rate (BER), and should be distant enough from the backscatter in order to allow the intended receiver to correctly extricate the useful signal. This is achieved designing communication waveforms that reside in (or very close to) the passband of the incident radar illumination, temporally (fast-time phase and amplitude) modulating them in order to possess a manageable level of correlation with the radar scattering. Further developments of the proposed approach are also presented in [3], where two notable enhancements consist in the assessment of the benefits of time-reversal for multipath mitigation and a combined two-stage detection/waveform classification scheme for destination receiver to self-synchronize without the need for prior cueing.

Intuitively, a tradeoff exists between the desire of ensuring a low SER and keeping a “low profile” in the communication. In fact, from one hand, in order to ensure that the embedded

Manuscript received 5 Nov. 2014; revised 19 Feb. 2015; accepted 26 Apr. 2015. The associate editor coordinating the review of this manuscript and approving it for publication was Prof. S. Blunt.

Part of this paper was presented at the 2015 IEEE International Radar Conference (RadarConf'15), Arlington (VA), US, May 2015 (see [1]).

D. Ciuonzo and A. De Maio are with the Università degli Studi di Napoli “Federico II”, Dipartimento di Ingegneria Elettrica e Tecnologie dell’Informazione, Via Claudio 21, I-80125 Napoli, Italy. E-mail: domenico.ciuonzo@ieee.org, ademai@unina.it.

G. Foglia and M. Piezzo are with ELETTRONICA S.p.A., Via Tiburtina Valeria, Km 13.700, I-00131 Roma, Italy. E-mail: goffredo.foglia@gmail.com, marco.piezzo@elt.it.

signal is LPI, the power injected by the tag has to be kept adequately below the ambient scattering level, and the correlation with the backscatter has to be sufficiently high; on the other hand, in order to guarantee satisfying communication error performance, a certain Signal-to-Interference Ratio (SIR) has to be achieved, and a suitable separation from the backscatter interference has to be assured. Therefore, following the hint of [2], in the present paper, we propose an intrapulse REM communication design procedure based on the joint optimization of the two aforementioned (conflicting) objectives; namely, we aim at producing weakly-correlated symbols capable of maximizing the SIR and minimizing the probability of intercept. The resulting waveform design problem can be cast into a non-convex multi-objective optimization. The problem is solved with the help of the so-called “scalarization technique”, i.e. the original vectorial problem is reduced into a scalar one via the use of the Pareto-optimal theory [14], [15], [16]. We prove that optimal points of the scalarized problem can be always found exploiting hidden convexity through the use of semidefinite programming and the rank-one decomposition theorems [17], [18]. Then, the proposed signals are chosen as Pareto-optimal points of the previously mentioned multi-objective optimization problem. The proposed approach can be seen as a general framework for REM waveform design and includes, as special instances, the simple (but yet effective) waveform designs provided in [2]. Notice that, in [2], it is shown that satisfactory SER values can be achieved suitably canceling the clutter contribution in the dominant portion of the eigenspectrum; this task is accomplished via a Decorrelating Filter (DF) since, in that case, the standard matched coherent receiver does not ensure an adequately low communication error rate. Conversely, as it will be shown later, the proposed approach attains interesting SER behaviors even when a Matched Filter (MF) is employed.

The rest of the paper is organized as follows. In Sec. II, we introduce the received signal model while in Sec. III we discuss the figure of merits to optimize. In Sec. IV, we formulate the waveform design problem, and present the algorithm providing Pareto-optimal waveforms. In Sec. V, we assess the performance of the proposed method also in comparison with the intrapulse REM communication techniques of [2]. Finally, in Sec. VI, we draw conclusions and outline possible future

research tracks; proofs are deferred to the Appendices¹.

II. SYSTEM MODEL

We consider the same model as in [2]. Precisely, let $s(t)$, $t \in [0, T]$, be the complex-baseband (with bandwidth B) of the transmit radar waveform illuminating a given area. After filtering, by sampling $s(t)$ at the Nyquist rate (i.e., B complex samples/second), a tag would obtain a discrete representation of the radar waveform, collected in $N \approx BT$ complex samples. However, at Nyquist rate, the radar waveform fully occupies the unambiguous bandwidth, thus leaving no spectral region where the symbol could be embedded.

Therefore, in order to acquire additional design Degrees-Of-Freedom (DOFs), the tag oversamples the incident wave at a rate of MB complex samples/second, with $M > 1$ being the oversampling factor: by doing so, additional spectrum can be exploited so as to earn a new covert region where the communication signal can be embedded. An example is herein given in **Fig. 1a**, where the amplitude spectrum of $s(t)$ for a real-valued Linearly Frequency Modulated (LFM) signal with one-sided bandwidth 750 kHz and duration $T = 133 \mu\text{s}$ is shown. The oversampling factor is set to $M = 2$, so that the useful bandwidth is actually doubled; notice that this operation makes available a new frequency region in the spectral tail of the oversampled sequence. Of course, by properly setting M , it is possible to decide how much additional spectral space (viz. DOFs, cf. **Fig. 1b**) can be made available at the tag².

Let $\mathbf{s} \triangleq [s(1) \ s(2) \ \dots \ s(MN)]^T$ be the column vector containing the MN samples. As shown in [2], a discrete representation of the radar backscattering model involves the convolution of the discretized sequence \mathbf{s} with the discretized version of the aggregate ambient scattering, which can be alternatively expressed in terms of the matrix multiplication in Eq. (1), where $\mathbf{x} \in \mathbb{C}^{(2MN-1) \times 1}$ contains the range samples of the aggregate ambient radar scattering, and $\mathbf{S} \in \mathbb{C}^{MN \times (2MN-1)}$ is the matrix accounting for the shifted versions of the illuminating radar waveform. Also, let \mathbf{c}_k , $k = 1, \dots, K$, be the k -th devised embedded symbol. Therefore, the discretized signal (when k -th waveform is transmitted) at the (intentional

¹*Notation* - We use boldface for vectors \mathbf{a} (lower case), and matrices \mathbf{A} (upper case). The n -th element of \mathbf{a} and the (m, ℓ) -th entry of \mathbf{A} are denoted by $a(n)$ and $\mathbf{A}(m, \ell)$, respectively. The transpose, conjugate, Hermitian, Euclidean norm, real part and trace operators are denoted by the symbols $(\cdot)^T$, $(\cdot)^*$, $(\cdot)^\dagger$, $\|\cdot\|$, $\Re\{\cdot\}$ and $\text{tr}(\cdot)$ respectively. \mathbf{I} and $\mathbf{0}$ denote the identity matrix and the matrix with zero entries (when not underlined through a subscript, their size will be easily understood from the context), respectively. \mathbb{R}^N , \mathbb{C}^N , and \mathbb{H}^N are the sets of N -dimensional vectors of real numbers, the sets of N -dimensional vectors of complex numbers, and $N \times N$ Hermitian matrices, respectively. Given a vector $\mathbf{a} \in \mathbb{C}^N$, $\text{diag}(\mathbf{a})$ indicates the N -dimensional diagonal matrix whose i -th diagonal element is $a(i)$, $i = 1, \dots, N$. The curled inequality symbol \succeq (and its strict form \succ) is used to denote generalized matrix inequality: for any $\mathbf{A} \in \mathbb{H}^N$, $\mathbf{A} \succeq \mathbf{0}$ (resp. $\mathbf{A} \succ \mathbf{0}$) means that \mathbf{A} is a positive semidefinite (resp. positive definite) matrix. $\mathcal{R}(\mathbf{X})$ denotes the range space of the matrix \mathbf{X} . For any $x \in \mathbb{C}$, $|x|$ represents its modulus. The letter j denotes the imaginary unit (i.e. $j = \sqrt{-1}$). $\mathbb{E}[\cdot]$ and $\text{var}[\cdot]$ denote the statistical expectation and variance, respectively. Furthermore, $\mathcal{CN}(\mathbf{0}, \mathbf{R})$ denotes a complex-valued multivariate Gaussian pdf with zero mean vector and covariance \mathbf{R} . Finally, for any optimization problem \mathcal{P} , we denote with $v(\mathcal{P})$ its optimal value.

²Clearly, the oversampling factor M cannot be increased indefinitely, since constraints on both electromagnetic compatibility and simplicity in tag/intended receiver hardware design have to be met.

$$\mathbf{S}\mathbf{x} = \begin{bmatrix} s(MN) & s(MN-1) & \dots & s(1) & 0 & \dots & 0 \\ 0 & s(MN) & \dots & s(2) & s(1) & \dots & 0 \\ \vdots & \vdots & \ddots & \vdots & \ddots & \vdots & \vdots \\ 0 & 0 & \dots & s(MN) & s(MN-1) & \dots & s(1) \end{bmatrix} \mathbf{x}, \quad (1)$$

and/or unintentional) receiver can be expressed, after perfect timing synchronization, as the following $MN \times 1$ vector³:

$$\mathbf{y}_{rk} = \alpha \mathbf{c}_k + \beta \mathbf{S}\mathbf{x} + \mathbf{n}, \quad (2)$$

where $\alpha \in \mathbb{C}$ is the (unknown) echo amplitude (accounting for the transmit amplitude and channels propagation effects), $\beta \in \mathbb{R}^+$ subsumes the strength of the interference sources, and $\mathbf{n} \in \mathbb{C}^{MN \times 1}$ is the vector of the noise samples.

Without loss of generality, with reference to \mathbf{x} and \mathbf{n} , we draw out both the vectors from independent white Gaussian distributions, that is $\mathbf{x} \sim \mathcal{CN}(\mathbf{0}, \frac{1}{MN} \mathbf{I})$ and $\mathbf{n} \sim \mathcal{CN}(\mathbf{0}, \frac{1}{MN} \mathbf{I})$ in order to account for the average power of the embedded communication signal and that of the auto-interference directly in α and β , respectively. Indeed, by doing so, the input Signal-to-Noise Ratio (SNR) and SIR when k -th waveform is transmitted are given by:

$$\text{SNR}_k \triangleq \mathbb{E} \left[\|\alpha \mathbf{c}_k\|^2 \right] / \mathbb{E} \left[\|\mathbf{n}\|^2 \right] = |\alpha|^2 \|\mathbf{c}_k\|^2; \quad (3)$$

$$\text{SIR}_k \triangleq \mathbb{E} \left[\|\alpha \mathbf{c}_k\|^2 \right] / \mathbb{E} \left[\|\beta \mathbf{S}\mathbf{x}\|^2 \right] = \frac{|\alpha|^2 \|\mathbf{c}_k\|^2}{\beta^2 \|\mathbf{s}\|^2}. \quad (4)$$

III. PERFORMANCE MEASURES

In this section we focus on the key performance measures to optimize or control in the selection of the modulating code.

A. Output SIR

As already stated, it is necessary, for demodulation purposes at the intended receiver, to have the exact knowledge of the K possible communication symbols transmitted by the tag. Thus, a set of properly designed K filters, say \mathbf{w}_k , $k = 1, \dots, K$, are assumed at receiver side. Given the signal model (2), the normalized (output) SIR for the k -th REM communication waveform is:

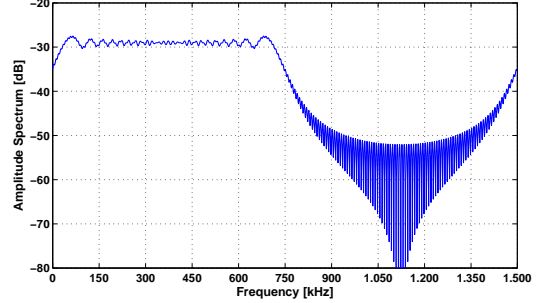
$$\text{SIR}_{o,k} \triangleq \frac{1}{MN} \frac{\mathbb{E} \left[|\mathbf{w}_k^\dagger \mathbf{c}_k|^2 \right]}{\mathbb{E} \left[|\mathbf{w}_k^\dagger \mathbf{S}\mathbf{x}|^2 \right]} = \frac{|\mathbf{w}_k^\dagger \mathbf{c}_k|^2}{\mathbf{w}_k^\dagger (\mathbf{S}\mathbf{S}^\dagger) \mathbf{w}_k}. \quad (5)$$

It is well known [19] that the filter maximizing (5) has the form $\mathbf{w}_k^* = (\mathbf{S}\mathbf{S}^\dagger)^{-1} \mathbf{c}_k$, which, after substitution, leads to the optimized k -th normalized SIR:

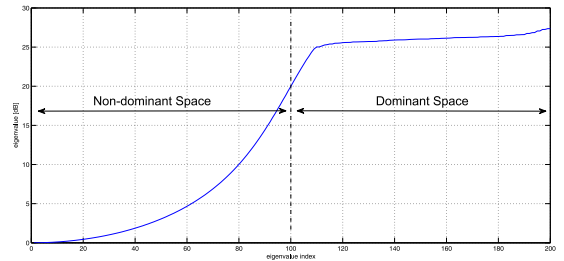
$$\text{SIR}_{o,k}^* = \mathbf{c}_k^\dagger (\mathbf{S}\mathbf{S}^\dagger)^{-1} \mathbf{c}_k. \quad (6)$$

The latter metric will be used as a performance measure to achieve low values of SER.

³Hereinafter we will use the notation \mathbf{y}_r when the actual symbol transmitted is not known at the receiver.



(a)



(b)

Figure 1: Complex baseband for a LFM signal with $B = 750$ kHz, $T = 133 \mu\text{s}$, $N = 100$, $M = 2$; a) amplitude spectrum; b) sorted eigenvalues of $\mathbf{S}\mathbf{S}^\dagger$.

B. Orthogonal projection

Using model (1), we can obtain a suited orthogonal basis for the waveforms design, computing the eigendecomposition of the correlation matrix of \mathbf{S} , i.e.

$$\mathbf{S}\mathbf{S}^\dagger = \mathbf{V}\mathbf{\Lambda}\mathbf{V}^\dagger, \quad (7)$$

where $\mathbf{\Lambda} = \text{diag} \left([\lambda_1 \ \lambda_2 \ \dots \ \lambda_{MN}]^T \right)$ is the diagonal matrix of the eigenvalues of $\mathbf{S}\mathbf{S}^\dagger$ (sorted in increasing magnitude, i.e. $\lambda_i \leq \lambda_{i+1}$), whereas $\mathbf{V} = [\mathbf{v}_1 \ \mathbf{v}_2 \ \dots \ \mathbf{v}_{MN}]$ contains the corresponding MN eigenvectors. Those belonging to the non-dominant space possess the least correlation with the ambient scatter; thus, they can be exploited to design our communication symbols, so as to lower the SER, at the price of a higher probability of intercept (since the communication symbols are not sufficiently “covered”). Following the so-called “Dominant Projection” (DP) approach of [2], we focus on projecting away the designed waveform \mathbf{c}_k from the dominant subspace.

To this end, let us define the following quantities:

- The eigendecomposition $\mathbf{S}_{P,k-1} \mathbf{S}_{P,k-1}^\dagger = \mathbf{V}_{P,k-1} \mathbf{\Lambda}_{P,k-1} \mathbf{V}_{P,k-1}^\dagger$, where $\mathbf{S}_{P,k-1} \triangleq [\mathbf{S} \ \mathbf{c}_1 \ \dots \ \mathbf{c}_{k-1}] \in \mathbb{C}^{MN \times (2MN+k-2)}$,

$k = 1, \dots, K$, is the matrix obtained comprising \mathbf{S} with the first $(k-1)$ -th communication waveforms, with the eigenvalues sorted in increasing magnitude (when $k = 1$, $\mathbf{S}_{P,0} = \mathbf{S}$, $\mathbf{V}_{P,0} = \mathbf{V}$, and $\mathbf{\Lambda}_{P,0} = \mathbf{\Lambda}$ hold).

- The specific index L of the eigenvectors belonging to the non-dominant space, but close enough to the dominant eigenspectrum. Indeed, L should not be chosen very large, as this would imply projection of part of the communication waveforms energy into the dominant space, thus leading to performance loss in terms of SER (and possibly interference to the radar receiver). On the other hand, L should not be taken very small, as this would cause a reduction in the DOFs available for the waveform design. For instance, a typical choice of L would be $L = (M-1)N$, i.e. considering the relevant energy of the radar waveform confined to highest N eigenvalues.
- $\mathbf{V}_{D,k-1} \triangleq [\mathbf{v}_{L-(k-1)+1} \ \dots \ \mathbf{v}_{MN}]$ contains the $(MN - L + k - 1)$ eigenvectors comprising the dominant space of $\mathbf{V}_{P,k-1}$.
- $\mathbf{P}_{k-1}^\perp \triangleq \mathbf{V}_{D,k-1} \mathbf{V}_{D,k-1}^\dagger$ and $\mathbf{P}_{k-1} \triangleq (\mathbf{I} - \mathbf{P}_{k-1}^\perp)$, $k = 1, \dots, K$, where \mathbf{P}_{k-1} projects any waveform away from the space defined by the $(MN - L + k - 1)$ vectors of the dominant space of $\mathbf{V}_{P,k-1}$.

Then, we search for waveforms complying with

$$\mathbf{P}_{k-1}^\perp \mathbf{c}_k = \mathbf{0}, \quad k = 1, \dots, K. \quad (8)$$

This strategy ensures weak correlation among the devised signals (viz. mutual orthogonality in the ideal case of a sharp decay of the dominant space and equal non-dominant space eigenvalues); moreover, due to the projection operation, the dominant space is involved as a whole, which confers to the design procedure an improved robustness with respect to other approaches which are based on the individual eigenvectors (as it has been pointed out and also shown in [2]). Before proceeding further, we remark that a slightly different procedure (which is also intended to ensure projection away from the dominant space) has been successively proposed in [3]. In this latter case, the design of k -th waveform is obtained as follows:

$$\mathbf{c}_k = \mathbf{P}_0 \mathbf{s}_k, \quad k = 1, \dots, K, \quad (9)$$

where the \mathbf{s}_k 's are suitably chosen seeds, i.e. drawn from a pseudo-random sequence [3]. However, in this manuscript, we only consider the first approach (i.e. Eq. (8)) for the following reason. Indeed, the first approach allows to keep the overall computational complexity of our proposed waveform design under control. Indeed, enforcing a simultaneous mutual orthogonality for all the waveforms, constructed according to Eq. (9), would lead to a (possibly non-convex) joint optimization for the *entire waveform set*, with corresponding dramatic increase of computational complexity. On the other hand, adoption of the metric in Eq. (8) allows for a natural sequential (and with reduced complexity) design of the waveforms \mathbf{c}_k , as it will be shown hereinafter.

C. Energy constraint

A critical aspect is represented by the energy radiated from the tag. Indeed, the power injected in the illuminated area has

to be properly tuned, so as to balance between an acceptable SER and a satisfying LPI. Moreover, another key aspect, from a practical point of view, is the actual energy source of the tag, since no battery or power source may actually be present to supply an active transmission (this may be the case of passive or semi-passive transponder, where a simple passive reflection occurs). Based on these reasons, we enforce an energy constraint, namely:

$$\|\mathbf{c}_k\|^2 = 1, \quad k = 1, \dots, K. \quad (10)$$

D. Similarity constraint

Aiming at increasing the covertness of the symbols, we enforce a spectral similarity with a prescribed unit-norm pseudo-random sequence (denoted here as $\mathbf{d}_{0,k}$) over the frequencies belonging to the spectral tail of the oversampled radar signal (e.g. $\approx [750, 1500]$ kHz in **Fig. 1a**); thus the communication signal will appear as a noise-like waveform (with a consequent likely flat spectrum) to a hostile eavesdropper scanning the whole spectrum in search for a transmission; the exchange of information between the transponder and the intended receiver will then proceed almost unnoticed. The similarity measure adopted here is $\|\mathbf{L} \mathbf{c}_k - \mathbf{L} \mathbf{d}_{0,k}\|^2$, with \mathbf{L} being a known matrix [20]. The structure of \mathbf{L} which enforces the desired spectral similarity is detailed hereinafter.

First, let $\widehat{\mathbf{W}}^z \triangleq [\mathbf{w}_1^T \ \mathbf{w}_2^T \ \dots \ \mathbf{w}_{\widehat{N}}^T]^T$ be the $\widehat{N} \times \widehat{N}$ (with $\widehat{N} > MN$) Discrete Fourier Transform (DFT) matrix whose \widehat{n} -th row ($\widehat{n} \in \{1, \dots, \widehat{N}\}$) corresponds to the “discrete” frequency $\nu_{\widehat{n}} \triangleq \frac{\widehat{n}-1}{\widehat{N}}$, that is

$$\mathbf{w}_{\widehat{n}} \triangleq \frac{1}{\sqrt{\widehat{N}}} \left[1 \quad e^{-j2\pi\nu_{\widehat{n}}} \quad \dots \quad e^{-j2\pi\nu_{\widehat{n}}(\widehat{N}-1)} \right]. \quad (11)$$

The aforementioned DFT matrix is applied here to the zero-padded waveforms $\mathbf{c}_k^z \triangleq [\mathbf{c}_k^T \ 0 \ \dots \ 0]^T \in \mathbb{C}^{\widehat{N} \times 1}$ and $\mathbf{d}_{0,k}^z \triangleq [\mathbf{d}_{0,k}^T \ 0 \ \dots \ 0]^T \in \mathbb{C}^{\widehat{N} \times 1}$, to allow a finer spectral shaping (clearly $(\widehat{N} - MN)$ denotes the number of appended zeros). Also, we underline that $\mathbf{c}_k^z = \bar{\mathbf{S}}_F \mathbf{c}_k$ and $\mathbf{d}_{0,k}^z = \bar{\mathbf{S}}_F \mathbf{d}_{0,k}$ hold, with $\bar{\mathbf{S}}_F \triangleq [\mathbf{I} \ 0]^T$ being a $\widehat{N} \times MN$ selection matrix.

The similarity constraint is here enforced only on a subset of $F < \widehat{N}$ discrete frequencies corresponding to the additional tail skirt of the backscattered radar signal spectrum⁴. This operation is formally expressed via the linear operator $\widehat{\mathbf{W}}^s \triangleq (\mathbf{S}_F \widehat{\mathbf{W}}^z)$ applied to the generic zero-padded waveform, where \mathbf{S}_F denotes a $F \times \widehat{N}$ row-selection matrix, e.g. $\mathbf{S}_F \triangleq [\mathbf{0} \ \mathbf{I}]$. Therefore, based on $\widehat{\mathbf{W}}^s$ definition, we can formulate the similarity constraint as

$$\|\widehat{\mathbf{W}}^s \mathbf{c}_k^z - \widehat{\mathbf{W}}^s \mathbf{d}_{0,k}^z\|^2 \leq \epsilon \quad k = 1, \dots, K, \quad (12)$$

where $\epsilon \geq 0$ is a tunable similarity parameter. Eq. (12) can be also equivalently expressed in terms of the non-padded waveforms as:

$$\|\widehat{\mathbf{W}} \mathbf{c}_k - \widehat{\mathbf{W}} \mathbf{d}_{0,k}\|^2 \leq \epsilon \quad k = 1, \dots, K, \quad (13)$$

⁴A reasonable choice for F is given by the approximate number of discrete frequencies not occupied by the radar signal, that is $F \approx \left(\frac{M-1}{M}\right) \widehat{N}$.

where $\widehat{\mathbf{W}} \triangleq (\mathbf{S}_F \widehat{\mathbf{W}}^z \bar{\mathbf{S}}_F) \in \mathbb{C}^{F \times MN}$ represents the matrix which weights only selected frequencies and non-zero samples. Finally, we show that $\epsilon \in [0, 4)$. Indeed, an upper bound to the left hand side of Eq. (12) is obtained as

$$\begin{aligned} \|\widehat{\mathbf{W}}^s \mathbf{c}_k^z - \widehat{\mathbf{W}}^s \mathbf{d}_{0,k}^z\|^2 &\leq \left(\|\widehat{\mathbf{W}}^s \mathbf{c}_k^z\| + \|\widehat{\mathbf{W}}^s \mathbf{d}_{0,k}^z\| \right)^2 \\ &< (\|\mathbf{c}_k^z\| + \|\mathbf{d}_{0,k}^z\|)^2 = 4 \end{aligned} \quad (14)$$

where first line follows from triangle inequality and second inequality is achieved only when both \mathbf{c}_k^z and $\mathbf{d}_{0,k}^z$ are aligned in the direction of the maximum (unit) eigenvalues of the matrix $\Psi \triangleq \left((\widehat{\mathbf{W}}^z)^\dagger (\mathbf{S}_F^\dagger \mathbf{S}_F) \widehat{\mathbf{W}}^z \right)$. Indeed, the aforementioned matrix has the eigenvalue matrix corresponding to $\mathbf{S}_F^\dagger \mathbf{S}_F$ (we recall that $\widehat{\mathbf{W}}^z$ is a unitary matrix); therefore there will be F orthogonal directions associated to the unit eigenvalue.

E. LPI metric

In [2], a simple metric is introduced to ascertain how accurately a (intentional or unintentional) receiver, with some prior knowledge on the radar emission $s(t)$ and the oversampling factor M , would be able to extract the symbol embedded within the radar backscatter. The key point is represented by the definition of the projection matrix $\tilde{\mathbf{P}}_\ell \triangleq (\mathbf{I} - \mathbf{V}_\ell \mathbf{V}_\ell^\dagger)$ for each $\ell \in \{1, \dots, MN\}$, where $\mathbf{V}_\ell \in \mathbb{C}^{MN \times \ell}$ is the matrix of eigenvectors corresponding to the ℓ largest eigenvalues⁵ of $\mathbf{S}\mathbf{S}^\dagger$ (cf. Eq. (7)). The assumption is that the hostile receiver is capable of projecting the received signal \mathbf{y}_{rk} over the ℓ -th projection matrix $\tilde{\mathbf{P}}_\ell$, getting the ℓ -th projection residue $\mathbf{z}_k^\ell \triangleq (\tilde{\mathbf{P}}_\ell \mathbf{y}_{rk})$; by doing so, it is possible to define the normalized correlation with the n -th communication waveform as

$$\eta_{n,k}^\ell \triangleq \frac{|\mathbf{c}_n^\dagger \mathbf{z}_k^\ell|}{\|\mathbf{c}_n\| \|\mathbf{z}_k^\ell\|} \quad \ell = 1, \dots, MN - 1, \quad (15)$$

where $|\mathbf{c}_n^\dagger \mathbf{z}_k^\ell| = |\alpha \mathbf{c}_n^\dagger \tilde{\mathbf{P}}_\ell \mathbf{c}_k + \beta \mathbf{c}_n^\dagger \tilde{\mathbf{P}}_\ell \mathbf{S}\mathbf{x} + \mathbf{c}_n^\dagger \tilde{\mathbf{P}}_\ell \mathbf{n}|$. Though not directly connected with the probability of intercept, Eq. (15) still represents a viable tool to figure out how accurately the communication waveform (embedded in the radar backscattering) can be extracted by a eavesdropper. Precisely, when $\eta_{n,k}^\ell$ (for a given projection index ℓ) gets higher values, we may infer that \mathbf{c}_n has a higher similarity with the waveform embedded in the received signal. In fact, first of all notice that, by construction, the signal \mathbf{c}_n is bounded to possess a partial correlation with the ambient backscatter; however, at the same time, it is designed so as to increase the SIR level at the receiver side, which basically is tantamount to enhancing the useful component with respect to the backscattering disturbance term: hence, it is fair to expect the correlation level with the residue $\tilde{\mathbf{P}}_\ell \mathbf{S}\mathbf{x}$ (which somehow encompasses the backscatter) to be non-null but yet sufficiently limited. Similarly, due to the independence of the radar transmission from the white thermal noise, we reasonably guess that the correlation between \mathbf{c}_n and the residue $\tilde{\mathbf{P}}_\ell \mathbf{n}$ is quite small. Therefore, with reference to the proposed design technique, our assumption is that the correlation between the signal \mathbf{c}_n

⁵Notice that, when $\ell = MN$, $\tilde{\mathbf{P}}_{MN} = \mathbf{0}$, hence we do not consider this projection index.

and the residue $\tilde{\mathbf{P}}_\ell \mathbf{c}_k$ has a greater impact, over the actual value of the correlation coefficient $\eta_{n,k}^\ell$, than the other two aforementioned components⁶. Given the orthogonal projection involved in (8), the mutual correlation between \mathbf{c}_n and the residue $\tilde{\mathbf{P}}_\ell \mathbf{c}_k$, for $k \neq n$ and $\ell = 1, \dots, MN - 1$, is designed to be extremely low. Consequently, we infer the correlation index $\eta_{n,k}^\ell$ to be quite small for $k \neq n$, for all $\ell = 1, \dots, MN - 1$, at least when $k \neq n$; nevertheless, this supposition may be no longer true when $k = n$. Therefore, in order to lower the correlation index $\eta_{n,n}^\ell$, we aim at *minimizing* the quadratic form $\mathbf{c}_n^\dagger \tilde{\mathbf{P}}_\ell \mathbf{c}_n$ for all $\ell = 1, \dots, MN - 1$.

Another useful interpretation of the proposed criterion is given by considering a different intercept metric proposed in [3], which is based on the detection of the communication process. More specifically, for the following hypothesis testing problem

$$\begin{cases} \mathcal{H}_0 : & \mathbf{y} = \beta \mathbf{S}\mathbf{x} + \mathbf{n} \\ \mathcal{H}_k : & \mathbf{y} = \mathbf{y}_{rk} = \alpha \mathbf{c}_k + \beta \mathbf{S}\mathbf{x} + \mathbf{n} \end{cases} \quad (16)$$

the authors of [3] define the intercept metric statistic:

$$\varepsilon_\ell \triangleq (\mathbf{y}^\dagger \tilde{\mathbf{P}}_\ell \mathbf{y}) \quad (17)$$

which is then compared to a suitable threshold for implementing a detection test at the non-intended receiver. While it is hard to give a complete statistical characterization of Eq. (17), we can give an insight based on a characterization up to the second order. Indeed, it can be shown that the mean values under the different hypotheses are given by:

$$\mathbb{E}[\varepsilon_\ell | \mathcal{H}_0] = \frac{\beta^2}{MN} \sum_{i=1}^{MN-\ell} \lambda_i + \frac{MN-\ell}{MN}, \quad (18)$$

$$\mathbb{E}[\varepsilon_\ell | \mathcal{H}_k] = |\alpha|^2 \mathbf{c}_k^\dagger \tilde{\mathbf{P}}_\ell \mathbf{c}_k + \frac{\beta^2}{MN} \sum_{i=1}^{MN-\ell} \lambda_i + \frac{MN-\ell}{MN}, \quad (19)$$

where λ_i are the (sorted) eigenvalues of Λ , while the variances are given by:

$$\text{var}[\varepsilon_\ell | \mathcal{H}_0] = \frac{1}{(MN)^2} \text{tr} \left[\tilde{\mathbf{P}}_\ell (\beta^2 \mathbf{S}\mathbf{S}^\dagger + \mathbf{I})^2 \right]; \quad (20)$$

$$\begin{aligned} \text{var}[\varepsilon_\ell | \mathcal{H}_k] &= \frac{1}{(MN)^2} \text{tr} \left[\tilde{\mathbf{P}}_\ell (\beta^2 \mathbf{S}\mathbf{S}^\dagger + \mathbf{I})^2 \right] + \\ &\quad \frac{2|\alpha|^2}{MN} \mathbf{c}_k^\dagger \tilde{\mathbf{P}}_\ell (\beta^2 \mathbf{S}\mathbf{S}^\dagger + \mathbf{I}) \tilde{\mathbf{P}}_\ell \mathbf{c}_k. \end{aligned} \quad (21)$$

Therefore, based on the above results, k normal (or modified) deflection measures [21] can be obtained as:

$$D_{0,k} \triangleq \frac{\{\mathbb{E}[\varepsilon_\ell | \mathcal{H}_k] - \mathbb{E}[\varepsilon_\ell | \mathcal{H}_0]\}^2}{\text{var}[\varepsilon_\ell | \mathcal{H}_0]} \quad (22)$$

$$D_{1,k} \triangleq \frac{\{\mathbb{E}[\varepsilon_\ell | \mathcal{H}_k] - \mathbb{E}[\varepsilon_\ell | \mathcal{H}_0]\}^2}{\text{var}[\varepsilon_\ell | \mathcal{H}_k]} \quad (23)$$

⁶Of course, it is not intention of the authors to claim that this statement holds true for all the possible design approaches, since it clearly depends on the intrapulse modulation technique adopted. Still, our simulations demonstrate the validity of our intuition, at least with respect to the proposed methodology.

from which it can be inferred whether transmission of the embedded k -th waveform can be discerned or not at the non-intended (eavesdropping) receiver. Deflection measures have a long history [22] and, in specific cases (such as Gauss-Gauss shift-in-mean binary testing), they are directly linked to the statistical power of the test under consideration. Nonetheless, in more complicated models (as ours), their use is somewhat arbitrary, even if literature has shown their effectiveness in some cases. Indeed, the intuitive rationale is that low deflections correspond to a statistic from which it can be hardly inferred the true hypothesis only from its second order characterization. Since the explicit expressions are

$$D_{0,k} = \frac{\left(|\alpha|^2 \mathbf{c}_k^\dagger \tilde{\mathbf{P}}_\ell \mathbf{c}_k\right)^2}{\text{var}[\varepsilon_\ell | \mathcal{H}_0]}, \quad (24)$$

$$D_{1,k} = \frac{\left(|\alpha|^2 \mathbf{c}_k^\dagger \tilde{\mathbf{P}}_\ell \mathbf{c}_k\right)^2}{\text{var}[\varepsilon_\ell | \mathcal{H}_0] + \frac{2|\alpha|^2}{MN} \mathbf{c}_k^\dagger \tilde{\mathbf{P}}_\ell (\beta^2 \mathbf{S}\mathbf{S}^\dagger + \mathbf{I}) \tilde{\mathbf{P}}_\ell \mathbf{c}_k}, \quad (25)$$

it is apparent that minimization of $D_{i,k}$'s is achieved by keeping $\mathbf{c}_k^\dagger \tilde{\mathbf{P}}_\ell \mathbf{c}_k$ for each waveform as small as possible. Therefore, the proposed measure can also virtually avoid detection of established communication between the transmitter and the intended receiver.

IV. PROBLEM FORMULATION

The idea pursued in this paper is to sequentially design REM communication waveforms, under the orthogonal projection constraint in (8), which jointly optimize the SER performance (through SIR maximization) and the LPI behavior (via minimization of $\mathbf{c}_n^\dagger \tilde{\mathbf{P}}_\ell \mathbf{c}_n$, $\ell = 1, \dots, MN - 1$), with a spectral similarity to a known pseudo-random sequence $\mathbf{d}_{0,k}$, and an energy constraint.

Based on these reasons, we formulate our problem in terms of a non-convex multi-objective (with MN objectives) optimization for k -th waveform as [14]

$$\mathcal{P}_1 \triangleq \begin{cases} \max_{\mathbf{c}_k} & \left(\mathbf{c}_k^\dagger (\mathbf{S}\mathbf{S}^\dagger)^{-1} \mathbf{c}_k ; -\{\mathbf{c}_k^\dagger \tilde{\mathbf{P}}_\ell \mathbf{c}_k\}_{\ell=1}^{MN-1} \right) \\ \text{s.t.} & \mathbf{P}_{k-1}^\perp \mathbf{c}_k = \mathbf{0}, \quad \mathbf{c}_k^\dagger \mathbf{c}_k = 1, \\ & \|\widehat{\mathbf{W}} \mathbf{c}_k - \widehat{\mathbf{W}} \mathbf{d}_{0,k}\|^2 \leq \epsilon, \end{cases} \quad (26)$$

for $k = 1, \dots, K$. The interested reader may refer to [14, pp. 174-184] for an exhaustive introduction to the multi-objective optimization and the scalarization technique, whereas examples of the use of the Pareto-optimization theory for radar applications can be found in [23], [16], [24]. The main aspect is the possibility to get an optimal solution to the starting vectorial problem from an optimal solution of its scalarized version, once a suitable weight vector $\zeta \succ \mathbf{0}$ (i.e. a component-wise positive vector) has been defined. Precisely, let

$$\begin{cases} \min_{\mathbf{x}} & \mathbf{f}_0(\mathbf{x}) \\ \text{s.t.} & f_i(\mathbf{x}) \leq 0, \quad h_j(\mathbf{x}) = 0, \end{cases} \quad (27)$$

be our multi-objective optimization problem, where $\mathbf{x} \in \mathbb{R}^n$ is the optimization variable, $f_i(\mathbf{x})$, $i = 1, \dots, m$ and $h_j(\mathbf{x})$, $i = 1, \dots, p$ are respectively the i -th inequality constraint and the j -th equality constraint function, and $\mathbf{f}_0(\mathbf{x}) : \mathbf{x} \in$

$\mathbb{R}^n \rightarrow \mathbb{R}^q$ is the vector-valued objective function whose q components $F_1(\mathbf{x}), \dots, F_q(\mathbf{x})$ can be interpreted as q different scalar objectives, each of which we would like to minimize. Then, an optimal solution to the vectorial problem (also known as Pareto-optimal point) can be obtained through the following scalar problem

$$\begin{cases} \min_{\mathbf{x}} & \zeta^T \mathbf{f}_0(\mathbf{x}) \\ \text{s.t.} & f_i(\mathbf{x}) \leq 0, \quad h_j(\mathbf{x}) = 0, \end{cases} \quad (28)$$

where the components of the weight vector $\zeta \triangleq [\zeta_1, \dots, \zeta_q]^T$ define the mutual weights given to each of the scalar objectives in the optimization procedure.

Following these guidelines, \mathcal{P}_1 can be thus reduced into the following scalarized form

$$\mathcal{P}_2 \triangleq \begin{cases} \max_{\mathbf{c}_k} & \mathbf{c}_k^\dagger \left(\frac{\zeta_1}{\lambda_{\max}(\mathbf{R})} \mathbf{R} - \frac{\zeta_2}{\lambda_{\max}(\tilde{\mathbf{P}})} \tilde{\mathbf{P}} \right) \mathbf{c}_k \\ \text{s.t.} & \mathbf{P}_{k-1}^\perp \mathbf{c}_k = \mathbf{0}, \quad \mathbf{c}_k^\dagger \mathbf{c}_k = 1, \\ & \|\widehat{\mathbf{W}} \mathbf{c}_k - \widehat{\mathbf{W}} \mathbf{d}_{0,k}\|^2 \leq \epsilon, \end{cases} \quad (29)$$

where $\frac{\zeta_1}{\lambda_{\max}(\mathbf{R})} > 0$ and $\frac{\zeta_2}{\lambda_{\max}(\tilde{\mathbf{P}})} > 0$ represent the weights, $\mathbf{R} \triangleq (\mathbf{S}\mathbf{S}^\dagger)^{-1}$ and $\tilde{\mathbf{P}} \triangleq \sum_{\ell=1}^{MN-1} \tilde{\mathbf{P}}_\ell$.

First Remark: it is worth pointing out that, in formulating \mathcal{P}_2 , we have implicitly assigned the same weight ζ_2 to the last $(MN - 1)$ components of the vectorial objective function. Namely, $\zeta = [\zeta_1 \quad \zeta_2 \quad \dots \quad \zeta_2]^T \in \mathbb{R}^{MN}$, so that:

$$\zeta^T \begin{bmatrix} \mathbf{c}_k^\dagger \mathbf{R} \mathbf{c}_k & -\mathbf{c}_k^\dagger \tilde{\mathbf{P}}_1 \mathbf{c}_k & \dots & -\mathbf{c}_k^\dagger \tilde{\mathbf{P}}_{MN-1} \mathbf{c}_k \end{bmatrix}^T = \mathbf{c}_k^\dagger \left[\zeta_1 \mathbf{R} - \zeta_2 \tilde{\mathbf{P}} \right] \mathbf{c}_k \quad (30)$$

We underline that the aforementioned weight set restriction in \mathcal{P}_2 is only made for the sake of simplicity and based on the assumption that, in absence of any knowledge on the dominant space, an interceptor should reasonably give equal confidence to all the presumed non-dominant spaces $\tilde{\mathbf{P}}_\ell$. Indeed, the proposed optimization approach straightforwardly applies also in the general case $\zeta \succ \mathbf{0}$. Equally important, we point out that the scalar objectives in Eq. (26) are not all concave (actually the normalized SIR is a convex function) and also the unitary energy constraint is not affine. Consequently, the multi-objective optimization under investigation (and consequently the scalarized problem) is not concave. Therefore we cannot claim that, by varying $\zeta \succ \mathbf{0}$ (in our specific case $\zeta_1 > 0$ and $\zeta_2 > 0$), we obtain the entire Pareto trade-off surface for the multi-objective (two-objective) optimization considered. Nonetheless, on the converse, the optimal points found for the scalarized problem under investigation *all belong to the Pareto frontier* [14], and are thus exploited in this study for the design of waveform \mathbf{c}_k .

Second Remark: We point out that considering all the $\mathbf{c}_k^\dagger \tilde{\mathbf{P}}_\ell \mathbf{c}_k$ in the multi-objective optimization \mathcal{P}_1 in Eq. (26) (and with the same weight ζ_2 in \mathcal{P}_2) is very important in order to ensure a reasonable LPI behaviour. In fact, it can be shown that the second term in Eq. (30), that is $\zeta_2 \mathbf{c}_k^\dagger \left[\sum_{\ell=1}^{MN-1} \tilde{\mathbf{P}}_\ell \right] \mathbf{c}_k$, can be rewritten as

$$\zeta_2 \sum_{t=1}^{MN-1} (MN - t) |\mathbf{v}_t^\dagger \mathbf{c}_k|^2; \quad (31)$$

which highlights that the terms $|v_t^\dagger c_k|^2$ in the sum (we underline that each term corresponds to the amount of energy of waveform c_k projected in t -th DOF) are not equally weighted and, more specifically, higher confidence (which implies a higher penalization) is given to DOFs associated to smaller λ_t 's. Those are the DOFs where waveform "masking" under the radar backscatter energy is less effective. Finally, we observe that an extremely dominating LPI behaviour (viz ζ_2 is very high) in the overall objective could lead to an excessive allocation of generic waveform energy to the DOFs with higher values λ_t . In such a case, even though the radar backscatter energy may be significant, a peaked (detectable) spectrum could be observed from a simple spectral analysis, thus compromising the LPI behaviour with respect to such approach. In the latter case, enforcing a similarity constraint becomes very important and mitigates this issue.

Third Remark: It can be shown that for \mathcal{P}_1 the inequality constraint can be safely restricted to be $\epsilon \in [0, 2)$. Indeed the left hand side of Eq. (12) is rewritten as:

$$\begin{aligned} & \|\widehat{\mathbf{W}}^s c_k^z - \widehat{\mathbf{W}}^s d_{0,k}^z\|^2 = \\ & (c_k^z)^\dagger \Psi c_k^z + (d_{0,k}^z)^\dagger \Psi d_{0,k}^z - 2 \Re \{ (c_k^z)^\dagger \Psi d_{0,k}^z \} \end{aligned} \quad (32)$$

We then consider a generic feasible solution for $c_k^z = a_k$ of \mathcal{P}_1 , such that $\|\widehat{\mathbf{W}}^s a_k - \widehat{\mathbf{W}}^s d_{0,k}^z\|^2 \in [2, 4)$. It is not difficult to show that the vector $c_k^z = -a_k$ has the following properties: (i) it is also a feasible solution for \mathcal{P}_1 , (ii) all the objectives of \mathcal{P}_1 attain the same values as in the case of $c_k^z = a_k$ and more importantly (iii) $\|-\widehat{\mathbf{W}}^s a_k - \widehat{\mathbf{W}}^s d_{0,k}^z\|^2 \in [0, 2)$ (this readily follows from sign change of real part in Eq. (32)). Therefore, without loss of generality, we will consider $\epsilon \in [0, 2)$ in the following of the paper.

A waveform c_k optimizes \mathcal{P}_2 iff it is optimal for \mathcal{P}_3 , defined as

$$\mathcal{P}_3 \triangleq \begin{cases} \max_{c_k} & c_k^\dagger T(\gamma) c_k \\ \text{s.t.} & P_{k-1}^\perp c_k = \mathbf{0}, \quad c_k^\dagger c_k = 1, \\ & \|\widehat{\mathbf{W}} c_k - \widehat{\mathbf{W}} d_{0,k}\|^2 \leq \epsilon, \end{cases} \quad (33)$$

where $T(\gamma) \triangleq (\mathbf{R} - \gamma \widetilde{\mathbf{P}})$ and $\gamma \triangleq \frac{\zeta_2}{\zeta_1} \frac{\lambda_{\max}(\mathbf{R})}{\lambda_{\max}(\widetilde{\mathbf{P}})} > 0$. The aforementioned claim is evident since the objective functions of \mathcal{P}_2 and \mathcal{P}_3 are proportional and additionally the feasible sets are the same.

Due to the first constraint, there exists a waveform $\widehat{c}_k \in \mathbb{C}^{(L-k+1)}$ such that $c_k = U_{k-1} \widehat{c}_k$, where $P_{k-1} = U_{k-1} U_{k-1}^\dagger$ (i.e. the column matrix of eigenvectors associated to the projector P_{k-1}). Hence, \mathcal{P}_3 can be reformulated as

$$\begin{cases} \max_{\widehat{c}_k} & \widehat{c}_k^\dagger [U_{k-1}^\dagger T(\gamma) U_{k-1}] \widehat{c}_k \\ \text{s.t.} & \widehat{c}_k^\dagger \widehat{c}_k = 1, \quad \|\widehat{\mathbf{W}} U_{k-1} \widehat{c}_k - \widehat{\mathbf{W}} d_{0,k}\|^2 \leq \epsilon, \end{cases} \quad (34)$$

where we have exploited $U_{k-1}^\dagger U_{k-1} = \mathbf{I}$ in expressing concisely the equality constraint. Also, from inspection of (34), it is apparent that the similarity vector should be defined as $d_{0,k} \triangleq U_{k-1} d_k / \|U_{k-1} d_k\|$, with $d_k \in \mathbb{C}^{(L-k+1) \times 1}$ being a pseudo-random vector. Indeed, both the projection and the normalization operations involved in the definition of $d_{0,k}$ are necessary to make feasible the optimization problem, since the

similarity vector has to be a direction vector belonging to the same subspace of c_k . Problem (34) can be further recast as

$$\mathcal{P}_4 \triangleq \begin{cases} \max_{\widehat{c}_k} & \widehat{c}_k^\dagger [U_{k-1}^\dagger T(\gamma) U_{k-1}] \widehat{c}_k \\ \text{s.t.} & \widehat{c}_k^\dagger \widehat{c}_k = 1, \\ & \widehat{c}_k^\dagger [-U_{k-1}^\dagger \widehat{\mathbf{W}}^\dagger \widehat{\mathbf{W}} U_{k-1}] \widehat{c}_k + \\ & 2 \Re \left\{ [U_{k-1}^\dagger \widehat{\mathbf{W}}^\dagger \widehat{\mathbf{W}} d_{0,k}]^\dagger \widehat{c}_k \right\} + \\ & (\epsilon - d_{0,k}^\dagger \widehat{\mathbf{W}}^\dagger \widehat{\mathbf{W}} d_{0,k}) \geq 0. \end{cases} \quad (35)$$

Obviously, if \widehat{c}_k^* is optimal for \mathcal{P}_4 , then $c_k^* = U_{k-1} \widehat{c}_k^*$ is optimal for \mathcal{P}_2 , and viceversa. Hence, without loss of generality, we will focus on \mathcal{P}_4 hereinafter. In particular, let us consider the following equivalent (homogeneous) Quadratically Constrained Quadratic Programming (QCQP) reformulation:

$$\mathcal{P}_5 \triangleq \begin{cases} \max_{\widehat{c}_k, t} & \text{tr}(\mathbf{Q}_0 \mathbf{X}) \\ \text{s.t.} & \text{tr}(\mathbf{Q}_1 \mathbf{X}) \geq 0, \quad \text{tr}(\mathbf{Q}_2 \mathbf{X}) = 1, \\ & \text{tr}(\mathbf{Q}_3 \mathbf{X}) = 1, \\ & \mathbf{X} \triangleq \begin{bmatrix} \widehat{c}_k \widehat{c}_k^\dagger & t^* \widehat{c}_k \\ t \widehat{c}_k^\dagger & |t|^2 \end{bmatrix}, \end{cases} \quad (36)$$

where the matrices \mathbf{Q}_i are defined as follows:

$$\begin{aligned} \mathbf{Q}_0 & \triangleq \begin{bmatrix} U_{k-1}^\dagger T(\gamma) U_{k-1} & \mathbf{0} \\ \mathbf{0} & 0 \end{bmatrix}, \\ \mathbf{Q}_1 & \triangleq \begin{bmatrix} -U_{k-1}^\dagger \widehat{\mathbf{W}}^\dagger \widehat{\mathbf{W}} U_{k-1} & U_{k-1}^\dagger \widehat{\mathbf{W}}^\dagger \widehat{\mathbf{W}} d_{0,k} \\ (U_{k-1}^\dagger \widehat{\mathbf{W}}^\dagger \widehat{\mathbf{W}} d_{0,k})^\dagger & \epsilon - d_{0,k}^\dagger \widehat{\mathbf{W}}^\dagger \widehat{\mathbf{W}} d_{0,k} \end{bmatrix}, \\ \mathbf{Q}_2 & \triangleq \begin{bmatrix} \mathbf{I} & \mathbf{0} \\ \mathbf{0} & 0 \end{bmatrix}, \quad \mathbf{Q}_3 \triangleq \begin{bmatrix} \mathbf{0} & \mathbf{0} \\ \mathbf{0} & 1 \end{bmatrix}. \end{aligned} \quad (37)$$

Both \mathcal{P}_4 and \mathcal{P}_5 share the same optimal values (the proof is given in Appendix A), i.e. $v(\mathcal{P}_4) = v(\mathcal{P}_5)$.

Therefore, in order to obtain an optimal solution to \mathcal{P}_2 it suffices to focus on \mathcal{P}_5 . Precisely, we can find an optimal solution \mathbf{X}^* to \mathcal{P}_5 in two (computationally efficient) steps. The first step involves the solution of the following semidefinite programming problem [25], which is evidently the SemiDefinite Relaxation (SDR) of \mathcal{P}_5 obtained from dropping the rank-one constraint on \mathbf{X} :

$$\mathcal{P}_6 \triangleq \begin{cases} \max_{\mathbf{X}} & \text{tr}(\mathbf{Q}_0 \mathbf{X}) \\ \text{s.t.} & \text{tr}(\mathbf{Q}_1 \mathbf{X}) \geq 0, \quad \text{tr}(\mathbf{Q}_2 \mathbf{X}) = 1, \\ & \text{tr}(\mathbf{Q}_3 \mathbf{X}) = 1, \quad \mathbf{X} \succeq \mathbf{0}. \end{cases} \quad (38)$$

The second step consists in the application of a rank-one matrix decomposition theorem [17, Thm. 2.3] (reported in the following lemma) in order to obtain a vector $\mathbf{x}^* = [(z^*)^T \ y^*]^T$, where $\mathbf{x}^*(\mathbf{x}^*)^\dagger$ corresponds to a specific rank-one projection of the optimal solution to \mathcal{P}_6 , denoted here \mathbf{X}_{sdr} . This operation is denoted by $\mathbf{x}^* = \mathcal{D}(\mathbf{X}_{\text{sdr}}, \mathbf{Q}_0, \mathbf{Q}_1, \mathbf{Q}_2, \mathbf{Q}_3)$ hereinafter. Such theorem ensures (under certain assumptions, specified in the following) the existence (and gives a constructive procedure to build it) of a rank-one solution $\mathbf{x}^*(\mathbf{x}^*)^\dagger$, obtained starting from \mathbf{X}_{sdr} , which attains the same value of the objective and still satisfies all the constraints. Therefore, $\mathbf{x}^*(\mathbf{x}^*)^\dagger = \mathbf{X}^*$ holds.

Finally, an optimal solution for \mathcal{P}_3 is found as $\hat{\mathbf{c}}_k^* = \mathbf{z}^*/y^*$, and accordingly an optimal solution to \mathcal{P}_2 is obtained as $\mathbf{c}_k^* = \mathbf{U}_{k-1}\hat{\mathbf{c}}_k^*$.

Lemma 1. Let $\mathbf{X} \in \mathbb{H}^N$ ($N \geq 3$) be a non-zero $N \times N$ matrix such that $\mathbf{X} \succeq \mathbf{0}$ and let $\mathbf{A}_i \in \mathbb{H}^{N \times N}$, $i \in \{1, 2, 3, 4\}$, and suppose that $[\text{tr}(\mathbf{Y} \mathbf{A}_1) \ \cdots \ \text{tr}(\mathbf{Y} \mathbf{A}_4)]^T \neq \mathbf{0}$, for any non-zero matrix $\mathbf{Y} \in \mathbb{H}^N$, $\mathbf{Y} \succeq \mathbf{0}$. Then,

- if $\text{rank}(\mathbf{X}) \geq 3$, one can find, in polynomial time, a rank-one matrix $\mathbf{x}\mathbf{x}^\dagger$ such that \mathbf{x} (whose dependence is underlined as $\mathbf{x} = \mathcal{D}_1(\mathbf{X}, \mathbf{A}_1, \mathbf{A}_2, \mathbf{A}_3, \mathbf{A}_4)$) is in $\mathcal{R}(\mathbf{X})$, and

$$\mathbf{x}^\dagger \mathbf{A}_i \mathbf{x} = \text{tr}(\mathbf{X} \mathbf{A}_i), \quad i \in \{1, 2, 3, 4\}; \quad (39)$$

- if $\text{rank}(\mathbf{X}) = 2$, for any $\mathbf{z} \notin \mathcal{R}(\mathbf{X})$, one can find a rank-one matrix $\mathbf{x}\mathbf{x}^\dagger$ such that \mathbf{x} (whose dependence is underlined as $\mathbf{x} = \mathcal{D}_2(\mathbf{X}, \mathbf{A}_1, \mathbf{A}_2, \mathbf{A}_3, \mathbf{A}_4)$) is in the linear subspace spanned by $\{\mathbf{z}\} \cup \mathcal{R}(\mathbf{X})$, and

$$\mathbf{x}^\dagger \mathbf{A}_i \mathbf{x} = \text{tr}(\mathbf{X} \mathbf{A}_i), \quad i \in \{1, 2, 3, 4\}. \quad (40)$$

Remark: We recall that applicability of Lem. 1 requires both \mathcal{P}_6 and its dual to be *solvable* [17]. To this end, it suffices to show that there exists a pair $\{\hat{\mathbf{c}}_k, t\}$ which is strictly feasible for \mathcal{P}_5 , with one example represented by $\{\hat{\mathbf{c}}_k, t\} = \{\mathbf{U}_{k-1}^\dagger \mathbf{d}_{0,k}, 1\}$. Then, strict feasibility of \mathcal{P}_6 (i.e. the corresponding SDR) is ensured via construction of the matrix

$$\mathbf{X}_F \triangleq (1 - \xi) \mathbf{U}_c (\mathbf{e}_1 \mathbf{e}_1^\dagger) \mathbf{U}_c^\dagger + \frac{\xi}{L - k + 1} \mathbf{U}_c (\mathbf{I} - \mathbf{e}_1 \mathbf{e}_1^\dagger) \mathbf{U}_c^\dagger, \quad (41)$$

where we have denoted $\mathbf{e}_1 \triangleq [1 \ 0 \ \cdots \ 0]^T$ and

$$\mathbf{U}_c \triangleq \begin{bmatrix} \mathbf{U}_F & \mathbf{0} \\ \mathbf{1}^T & 1 \end{bmatrix}, \quad (42)$$

which is built starting from the unitary matrix $\mathbf{U}_F \triangleq [\hat{\mathbf{c}}_k \ \mathbf{u}_1 \ \cdots \ \mathbf{u}_{L-k}]$. It can be easily verified that $\mathbf{X}_F \succ \mathbf{0}$ and also complies with the equality constraints in \mathcal{P}_6 . Furthermore, the tunable parameter $\xi > 0$ in Eq. (41) can be made sufficiently small to satisfy the inequality constraint $\text{tr}(\mathbf{Q}_1 \mathbf{X}_F) > 0$. Differently, strict feasibility of the dual SDR, denoted here as \mathcal{DP}_6 , can be easily verified from its direct inspection:

$$\mathcal{DP}_6 \triangleq \begin{cases} \min_{y_1, y_2, y_3} & (y_2 + y_3) \\ \text{s.t.} & (-y_1 \mathbf{Q}_1 + y_2 \mathbf{Q}_2 + y_3 \mathbf{Q}_3 - \mathbf{Q}_0) \succeq \mathbf{0}, \\ & y_1 \geq 0 \end{cases} \quad (43)$$

It is apparent that proper combination (through y_2 and y_3) of \mathbf{Q}_2 and \mathbf{Q}_3 ensures positive definiteness and thus, strict feasibility.

Finally, in **Alg. 1** we summarize the (sequential) procedure leading to an optimal solution to \mathcal{P}_2 .

V. PERFORMANCE ANALYSIS

In the present section, we assess the reliability and the covertness of REM communication waveforms $\mathbf{c}_k^{\text{Alg1}}$, for $k = 1, \dots, K$, produced through **Alg. 1**, in terms of SER and Intercept Metric (IM).

Algorithm 1 Algorithm to solve the radar waveform design problem \mathcal{P}_2 .

Input: $L, M, \mathbf{S}, \mathbf{U}_{k-1}, \widehat{\mathbf{W}}, \mathbf{d}_{0,k}, \epsilon, \gamma$;

Output: An optimal solution \mathbf{c}_k^* to problem \mathcal{P}_2 ;

- 1) solve problem \mathcal{P}_6 , getting a solution \mathbf{X}_{sdr} ;
 - 2) find $\mathbf{x}^* = \mathcal{D}(\mathbf{X}_{\text{sdr}}, \mathbf{Q}_0, \mathbf{Q}_1, \mathbf{Q}_2, \mathbf{Q}_3)$; let $\mathbf{x}^* = [(z^*)^T \ y^*]^T$;
 - 3) set $\hat{\mathbf{c}}_k^* = \mathbf{z}^*/y^*$.
 - 4) return $\mathbf{c}_k^* = \mathbf{U}_{k-1}\hat{\mathbf{c}}_k^*$.
-

A. Simulation setup

For our comparison we consider a unitary norm LFM pulse as the incident radar signal, with a duration $T = 133 \mu\text{s}$, bandwidth $B = 750 \text{ kHz}$, and a chirp rate $K_s = (\frac{750}{133} \times 10^9) \text{ Hz/s}$; when sampled at Nyquist rate $f_s = B$, we obtain the following discrete-time representation of $s(t)$:

$$s(n) = \frac{1}{\sqrt{N}} e^{j2\pi \frac{K_s}{2} ((n-1)/f_s)^2}, \quad n = 1, \dots, N, \quad (44)$$

where $N = 100$. Differently, the signal is oversampled by the tag with a factor $M = 2$, thus resulting in additional DOFs. Clearly, an analogous discrete-time representation as Eq. (44) is obtained at the tag when substituting $f_s = MB$ and $N = 200$ samples. The number of communication waveforms (symbols) is set to $K = 4$ (2 bits). As explained in Sec. II, the ambient radar scatter \mathbf{x} and noise \mathbf{n} are modeled as $\mathbf{x} \sim \mathcal{CN}(\mathbf{0}, \frac{1}{MN} \mathbf{I})$ and $\mathbf{n} \sim \mathcal{CN}(\mathbf{0}, \frac{1}{MN} \mathbf{I})$, and the average power of the embedded communication signal, the ambient radar scatter (the interference), and the noise in (2) are each scaled to achieve the desired levels of SIR and SNR. Otherwise stated, given the received signal model \mathbf{y}_{rk} of (2), we consider $\alpha_k = \sqrt{\text{SNR}}$ and $\beta = \sqrt{\text{SNR}/\text{SIR}}$. Furthermore, we set $L = 100$. Finally, with reference to the similarity constraint in Eq. (13), we set $\hat{N} = 8MN$ and $F = 4MN + 6 = 806$, respectively.

For completeness of comparison, we report the SER and the interception curves for the following four design techniques:

- 1) the ‘‘Eigenvectors-As-Waveform’’ (EAW) approach of [2], where the K eigenvectors corresponding to the smallest K eigenvalues are used as communication symbols. Namely, $\mathbf{c}_k^{\text{EAW}} \triangleq \mathbf{v}_k$, $k = 1, \dots, K$, with $\mathbf{v}_1, \dots, \mathbf{v}_K$ being the eigenvectors associated with the K smallest eigenvalues.
- 2) the ‘‘Weighted-Combining’’ (WC) approach of [2], where the K symbols are drawn out properly weighting a set of L non-dominant eigenvectors with different weight vectors $\mathbf{b}_k \in \mathbb{C}^{L \times 1}$, $k = 1, \dots, K$, known only to the tag and the intended receiver. Namely, letting $\mathbf{V}_{ND} = [\mathbf{v}_1 \ \cdots \ \mathbf{v}_L]$, $\mathbf{c}_k^{\text{WC}} \triangleq \mathbf{V}_{ND} \mathbf{b}_k$, $k = 1, \dots, K$. In what follows, we draw $\mathbf{b}_k \sim \mathcal{CN}(\mathbf{0}, \mathbf{I})$, and \mathbf{c}_k^{WC} is scaled to have unitary norm.
- 3) the DP approach of [2], where the K waveforms are sequentially designed by ‘‘projecting away’’ from the (accumulated) whole dominant space a set of pseudo-random vectors $\mathbf{d}_k^{\text{DP}} \in \mathbb{C}^{MN \times 1}$, $k = 1, \dots, K$, available only at the tag and the intended receiver. Precisely,

$\mathbf{c}_k^{\text{DP}} \triangleq \mathbf{P}_{k-1} \mathbf{d}_k^{\text{DP}}$, $k = 1, \dots, K$. In the following, $\mathbf{d}_k^{\text{DP}} \sim \mathcal{CN}(\mathbf{0}, \mathbf{I})$, and \mathbf{c}_k^{DP} is scaled to have unitary norm.

- 4) the *minimum LPI* approach, where the K communication waveforms are devised so as to minimize the intercept metric (15) for all the projection matrices $\tilde{\mathbf{P}}_\ell$, $\ell = 1, \dots, MN - 1$. Namely, $\mathbf{c}_k^{\text{LPI}}$ is an optimal solution for the optimization problem⁷:

$$\mathcal{P}_{\text{LPI}} \triangleq \begin{cases} \min_{\mathbf{c}_k} & \mathbf{c}_k^\dagger \tilde{\mathbf{P}} \mathbf{c}_k \\ \text{s.t.} & \mathbf{P}_{k-1}^\perp \mathbf{c}_k = \mathbf{0}, \quad \mathbf{c}_k^\dagger \mathbf{c}_k = 1, \\ & \|\widehat{\mathbf{W}} \mathbf{c}_k - \widehat{\mathbf{W}} \mathbf{d}_{0,k}\|^2 \leq \epsilon, \end{cases} \quad (45)$$

where the matrix $\tilde{\mathbf{P}}$, accounting for the weighted sum of the projection matrices, is defined as in \mathcal{P}_2 .

As to the filtering strategy, following the hint of [2], we assume that the interder receiver may employ:

- a MF, i.e., $\mathbf{w}_k = \mathbf{c}_k$, $k = 1, \dots, K$;
- a DF⁸, i.e., $\mathbf{w}_k = (\mathbf{C}\mathbf{C}^\dagger)^{-1} \mathbf{c}_k$, $k = 1, \dots, K$, where $\mathbf{C} \triangleq [\mathbf{S} \mathbf{c}_1 \dots \mathbf{c}_K]$.

Given the received signal \mathbf{y}_r , at the receiver side an embedded communication symbol \bar{c} is extracted as

$$\bar{c} \triangleq \arg \max_{\{c_1, c_2, \dots, c_K\}} |\mathbf{w}_k^\dagger \mathbf{y}_r|. \quad (46)$$

Thus, for each of the aforementioned waveform design technique, the following experiments have been considered:

- for what concerns the evaluation of the SER performance, firstly we design 10 sets of K communication symbols⁹; then, for each set, we consider 10^5 independent identically distributed (iid) realizations of the noise and the interference impairments, which results in 10^5 iid instances of the received signal \mathbf{y}_{rk} . Aiming at a fair comparison, we use the same disturbance set for all the K symbols: by doing so, we intent to test their effectiveness under the same impairment conditions. For each of the $K \times 10^5$ realizations of the received signal, we apply the decision rule (46), and declare a successful transmission only when \bar{c} effectively equals the transmitted waveform (namely, the embedded communication symbol is correctly extracted). The SER performance is, hence, evaluated accordingly. Finally, the SER is averaged over the total number of available sets. The experiment is performed for three different values of SIR (that is, $\text{SIR} \in \{-40, -35, -30\}$ dB), assuming an SNR in $[-15, 0]$ dB.
- for what concerns the evaluation of the intercept metric (15), we first generate 10 different sets of K symbols¹⁰;

⁷Clearly, also \mathcal{P}_{LPI} can be solved optimally in an efficient way, similarly as for \mathcal{P}_2 .

⁸In what follows we do not report the performance for the filter which maximizes the SIR in Eq. (5), that is $\mathbf{w}_k = (\mathbf{S}\mathbf{S}^\dagger)^{-1} \mathbf{c}_k$. The reason is that *nearly identical* behaviour to the DF has been observed numerically in the considered scenarios.

⁹Different sets of K symbols correspond to different instances for the random vectors \mathbf{b}_k , \mathbf{d}_k^{DP} , and \mathbf{d}_k , respectively for WC, DP, and **Alg. 1** approaches. By iterating the experiment over a multitude of possible sets, we aim at reducing the variation of SER with respect to set selection.

¹⁰As for the SER evaluation, we iterate the experiment over a multitude of possible sets in order to reduce the variation of the intercept metric (15) with respect to set selection.

then, for each set, we consider 200 iid realizations of the noise and the interference components, and assume that the waveform corresponding to the index $k = 1$ is transmitted by the tag¹¹. This results in 200 realizations of the received signal $\mathbf{y}_{1r} = \alpha_1 \mathbf{c}_1 + \beta \mathbf{S}\mathbf{x} + \mathbf{n}$ for each of the 10 sets. The LPI behavior of the devised symbol is, therefore, estimated by ascertaining the intercept metric through Eq. (15) and averaging it over the total number of disturbance realizations and the total number of available sets. The experiment is performed assuming $\text{SIR} = -35$ dB and $\text{SNR} = -10$ dB.

B. Simulation results

In **Figs. 2, 3, and 4**, we analyze the SER vs. SNR for the symbols $\mathbf{c}_k^{\text{Alg1}}$, for different values of the similarity parameter ϵ and the Pareto weight γ (when either a MF or a DF is employed at the receiver side) and compare the results with those achieved by $\mathbf{c}_k^{\text{LPI}}$ (in **Figs. 2, 3, and 4**), $\mathbf{c}_k^{\text{EAW}}$ (in **Figs. 2**), \mathbf{c}_k^{WC} (in **Figs. 3**), and \mathbf{c}_k^{DP} (in **Figs. 4**). More specifically, **Figs. 2-a1, 2-b1, 2-c1, and 2-d1** refer to the MF, for $\epsilon = 0.01, 0.05, 0.1, \text{ and } 0.5$, respectively. Conversely, **Figs. 2-a2, 2-b2, 2-c2, and 2-d2** refer to the DF, for $\epsilon = 0.01, 0.05, 0.1, \text{ and } 0.5$, respectively. The same structure has been adopted for the plots shown in **Figs. 3** and **Figs. 4**. With reference to $\mathbf{c}_k^{\text{Alg1}}$, we report the results for $\gamma = 0$, $\gamma = 2$, and $\gamma = 2.3$, respectively.

A first inspection of the curves obtained with $\mathbf{c}_k^{\text{Alg1}}$ reveals that lower SER is achieved with small values of γ ; such behavior is a direct consequence of the mediative role of the Pareto weight between the two actors involved in the optimization problem. In fact, the importance of the *reliability* of the embedded communication over its *covertiness* grows considerably as γ is decreased (we recall that these features are represented respectively by the the maximization of the first component and the minimization of the remaining components of the vectorial optimization function of \mathcal{P}_1); hence, we expect higher interception probabilities to be swapped for lower SER values. Indeed, in the extreme case $(\gamma, \epsilon) = (0, 2)$, we expect that SER performance will attain those of EAW. This can be explained since in the mentioned scenario the similarity constraint is not active and $\gamma = 0$ implies sequential (output) SIR maximization, whose closed form solution is the EAW design itself.

This intuition is partially confirmed by a comparison of the results obtained for different similarity parameters. Indeed, the plots highlight the capability, of the proposed approach, to attain remarkable SER improvements (namely, to ensure more and more reliable communications) as ϵ increases, when $\gamma \in \{0, 2\}$. Conversely, when higher values of γ are adopted (for instance, $\gamma = 2.3$), the symbols $\mathbf{c}_k^{\text{Alg1}}$ experience a partial loss in terms of SER profiles (on behalf of more and more covert embedded transmissions), which becomes heavier as the similarity constraint is loosen. For instance, with reference to the MF, we can easily observe this effect by a comparison of **Figs. 2-a1, 2-b1, 2-c1, and 2-d1**; the same phenomenon occurs when a DF is employed (see **Figs.**

¹¹Indeed, it has been observed numerically that considering other waveforms in the set leads to similar behaviours in terms of intercept curves.

2-a2, **2-b2**, **2-c2**, and **2-d2**). This is not surprising, since relaxing the similarity constraint is tantamount to enlarging the feasible set: hence, additional DOFs are at disposal for the optimization procedure, which can be potentially exploited to further refine the most relevant components of the vectorial optimization function. Specifically, when the relative weight of the *interception* feature is more prominent (γ is large), we expect that the additional DOFs are spent to lower the interceptability of the transmission, of course to the detriment of its intelligibility. The inverse happens when the *reliability* characteristic assumes greater importance (γ is small): the error rates diminish since higher SIR values are attained, in response to the widening of the similarity set. On the other hand, when ϵ is taken to be very small, it is expected (as confirmed by simulations) that both c_k^{Alg1} and c_k^{LPI} design collapse to a DP design, since the similarity constraint enforces a strict similarity to noise-like waveforms which are made weakly-correlated and orthogonal to the dominant space (this is indeed the natural outcome of the constraint $P_{k-1}^\perp c_k = \mathbf{0}$, $k = 1, \dots, K$). From the analysis, we can also ascertain the effectiveness of the interference cancellation capability of the DF over the MF for all the considered waveform designs, since the former filtering strategy substantially outperforms the latter.

Furthermore, SER of EAW approach is identical with both MF and DF, and is lower than that achieved with **Alg. 1**. Indeed the symbols c_k^{EAW} exploit the eigenvectors possessing the least correlation with the ambient backscatter; hence, they are more easily “pulled out” from the received signal than c_k^{Alg1} (which are instead designed to exhibit a partial correlation with the ambient backscatter). Also, since each waveform c_k^{EAW} is associated to a distinct eigenvector of SS^\dagger , EAW does not get any profit from the cancellation (pre-whitening) capability provided by the DF (i.e. c_k^{EAW} already provide interference suppression). On the other hand, when $\gamma \in \{0, 2\}$, the proposed approach is comparable with, or totally outperforms, both WC and DP strategies in terms of reliability. This outcome can be easily explained noticing that, for the above values of γ , the SIR levels attained with the codes c_k^{Alg1} are still higher than those achieved by c_k^{WC} and c_k^{DP} . Therefore, even if all the three techniques possess a partial correlation with the ambient backscatter (in spite of EAW), the proposed waveform design still allows for easier extraction of the embedded symbol for the intended receiver. When $\gamma = 2.3$, we experience a SER loss with respect to EAW, WC, and DP approaches; as already highlighted, this loss is due to the existing trade-off between the SER profile and the covertness capability of the tag: we presume that this loss will be payed off with lower probabilities of interception. Finally, we observe that, when a MF is adopted, c_k^{LPI} achieves similar SER to c_k^{Alg1} for $\gamma = 2.3$; different situation occurs, instead, with the DF.

In **Figs. 5**, **6**, and **7**, we show the IM of the symbols c_k^{Alg1} , for $\epsilon \in \{0.01, 0.05, 0.1, 0.5\}$ and $\gamma \in \{0, 2, 2.3\}$, and compare the results with those obtained by the codes c_k^{LPI} (in **Figs. 5**, **6**, and **7**), c_k^{EAW} (in **Figs. 5**), c_k^{WC} (in **Figs. 6**), and c_k^{DP} (in **Figs. 7**). The trend of the proposed technique is in line with that displayed in the above analysis. Specifically, higher values of γ correspond to lower correlation values for waveform

1 obtained with **Alg. 1**, and the IM of c_k^{LPI} is approached in this case, which denotes the actual lower bound for the considered figure of merit (cf. **Fig. 5-a**). Hence, it is possible to prevent that an hostile eavesdropper could neither extract the embedded signal nor actually get aware of the transmission. From this point of view, our approach surpasses EAW, WC, and DP, substantially always ensuring lower correlation values when γ is sufficiently big. On the other hand, the covertness capabilities of the embedded communication worsen for smaller weights, since the SIR component is advantaged in the optimization procedure (however the IM is quite low, thus a covert conversation is still virtually possible). Moreover, the correlation values for waveforms 2, 3, and 4 are smaller: this implies that an intended receiver, provided a previous knowledge of the related symbols, would be easily able to discern which is the symbol embedded in the actual received signal, resorting to a coherent filtering.

By relaxing the similarity constraint (viz. increasing ϵ), this trend becomes more evident (cf. **Figs. 5-a**, **5-b**, **5-c**, and **5-d**). In particular, when $\gamma = 2.3$ the proposed procedure ensures a more covert transmission; differently, the reverse effect is displayed for $\gamma \in \{0, 2\}$, where slightly higher correlation values are obtained for all the waveforms. These results confirm our previous insight: worse SER profiles can be swapped for better intercept features by properly tuning the weight γ . Furthermore, by increasing the similarity parameter, more DOFs are obtained due to the enlargement of the feasible set, which are spent to emphasize, in the optimization problem, the property holding the greatest importance. As to the reference design technique, when γ is kept limited, **Alg. 1** basically outperforms EAW approach for all the settings of ϵ ; however, it displays a behavior comparable to those of WC and DP only when the similarity constraint is sufficiently tight ($\epsilon < 0.1$, for the case at hand), once again displaying the conflicting nature of the two actors involved in our optimization problem.

Summarizing, our analysis has shown that, by properly adjusting both the similarity level and the Pareto weight, the proposed design strategy proves to be better than, or at least comparable with, the EAW, the WC, and the DP approaches, in terms of covertness and reliability of a radar embedded communication between the tag and the intended receiver. Equally important, EAW, DP, WC and minimum LPI approaches *can be seen as special instances* of c_k^{Alg1} when γ and ϵ are set to “extreme” values, thus confirming the generality of the proposed waveform design framework.

C. Computational complexity

Finally, we discuss here the computational complexity of the proposed approach and of the other considered alternatives. Firstly, we observe that the heavier (in terms of complexity) step for the design of the waveform set of both EAW and WC approaches is represented by the eigendecomposition of the correlation matrix SS^\dagger . Thus their complexity is dominated by the term $O((MN)^3)$.

Secondly, the complexity of the DP approach is dominated by the K eigendecompositions required to project each waveform onto the (updated) non-dominant space. In

other words, for the k -th waveform, the eigendecomposition $\mathbf{S}_{P,k-1}\mathbf{S}_{P,k-1}^\dagger = \mathbf{V}_{P,k-1}\mathbf{\Lambda}_{P,k-1}\mathbf{V}_{P,k-1}^\dagger$ is evaluated, where $\mathbf{S}_{P,k-1} \triangleq [\mathbf{S} \ \mathbf{c}_1 \ \cdots \ \mathbf{c}_{k-1}] \in \mathbb{C}^{MN \times (2MN+k-2)}$. Therefore, its overall complexity is dominated by the term $\mathcal{O}(K(MN)^3)$.

Thirdly, we remark that the proposed approach will first require similar (in terms of complexity) eigendecompositions as the DP approach. Thus, the complexity required for the pre-processing of each sequential step is given by $\mathcal{O}((MN)^3)$. Also, the k -th sequential optimization has been proved to share a worst-case order computational complexity $\mathcal{O}((L-k+1)^{4.5} \log(1/\xi))$, (ξ being the desired accuracy for the solution of the SDR) [26]. Furthermore, a (lower) complexity $\mathcal{O}((L-k+1)^3)$ is required for application of the rank-one decomposition theorem [17]. Therefore, the computation of the entire waveform set requires a complexity of $\mathcal{O}(\sum_{k=1}^K (L-k+1)^{4.5} \log(1/\xi))$. Therefore, collecting all the terms provides:

$$\mathcal{O}\left(K(MN)^3 + \sum_{k=1}^K [(L-k+1)^{4.5} \log(\xi^{-1})]\right) \quad (47)$$

VI. CONCLUSIONS

In the present paper, we have focused on intrapulse REM communication, where the incident radar illumination is re-modulated, through an RF tag/transponder, into one of K information symbols. First, we have exploited the radar backscatter, so that the devised symbols would possess a certain correlation with the ambient electromagnetic environment, which ensures a certain stealthiness level to the transmission. Then, we have devised our communication waveforms in accordance to the following criterion: jointly constrained optimization of both the reliability of the transmission (through the maximization of the SIR) and the covertness of the communication (through the minimization of an intercept metric). The problem has been formulated in terms of a non-convex multi-objective optimization problem with two quadratic constraints. Hence, radar codes have been constructed as Pareto-optimal points of the aforementioned problem through the scalarization procedure. At the analysis stage, we have evaluated the performance of the new algorithm in terms of SER and LPI performance. The results have shown the capability of the proposed approach to suitably trade-off the reliability and the covertness features of the established communication.

Possible future research tracks might concern the extension of the framework to situations where it is also necessary to account for the multipath effects, and/or where it is necessary to force additional constraints on the structure of the radar waveform. Additionally, design of transmit-receive filters which account for the discovery of a tag transmission (as in [3]) and for possible timing uncertainties at the receiver will be object of future studies.

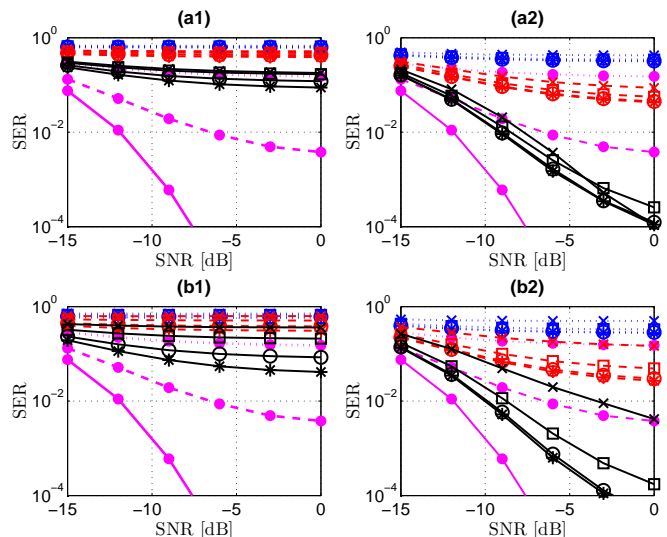


Figure 2: SER vs SNR (dB); SIR = -30 dB (continuous lines); SIR = -35 dB (dashed lines); SIR = -40 dB (dotted lines). EAW: \bullet -marked curves; **Alg. 1**, $\gamma = 0$: $*$ -marked curves; **Alg. 1**, $\gamma = 2$: \circ -marked curves; **Alg. 1**, $\gamma = 2.3$: \square -marked curves; **min. LPI**: \times -marked curves. **a1)** $\epsilon = 0.01$, MF; **a2)** $\epsilon = 0.01$, DF; **b1)** $\epsilon = 0.05$, MF; **b2)** $\epsilon = 0.05$, DF.

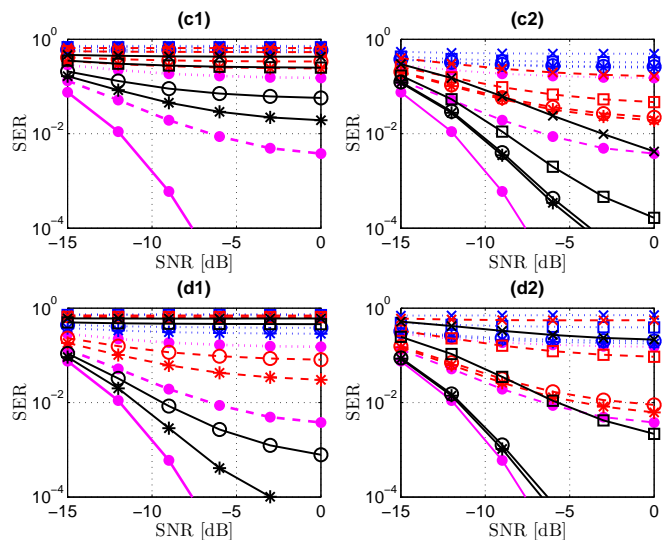


Figure 2: SER vs SNR (dB); SIR = -30 dB (continuous lines); SIR = -35 dB (dashed lines); SIR = -40 dB (dotted lines). EAW: \bullet -marked curves; **Alg. 1**, $\gamma = 0$: $*$ -marked curves; **Alg. 1**, $\gamma = 2$: \circ -marked curves; **Alg. 1**, $\gamma = 2.3$: \square -marked curves; **min. LPI**: \times -marked curves. **c1)** $\epsilon = 0.1$, MF; **c2)** $\epsilon = 0.1$, DF; **d1)** $\epsilon = 0.5$, MF; **d2)** $\epsilon = 0.5$, DF.

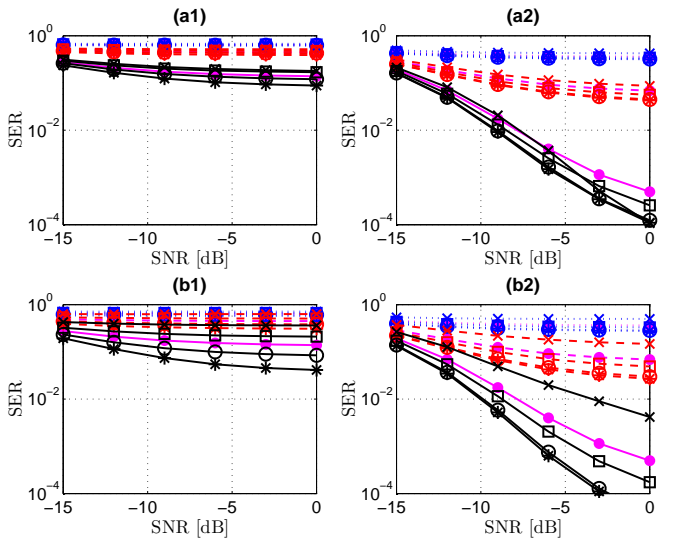


Figure 3: SER vs SNR (dB); SIR = -30 dB (continuous lines); SIR = -35 dB (dashed lines); SIR = -40 dB (dotted lines). WC: \bullet -marked curves; **Alg. 1**, $\gamma = 0$: $*$ -marked curves; **Alg. 1**, $\gamma = 2$: \circ -marked curves; **Alg. 1**, $\gamma = 2.3$: \square -marked curves; **min. LPI**: x -marked curves. **a1)** $\epsilon = 0.01$, MF; **a2)** $\epsilon = 0.01$, DF; **b1)** $\epsilon = 0.05$, MF; **b2)** $\epsilon = 0.05$, DF.

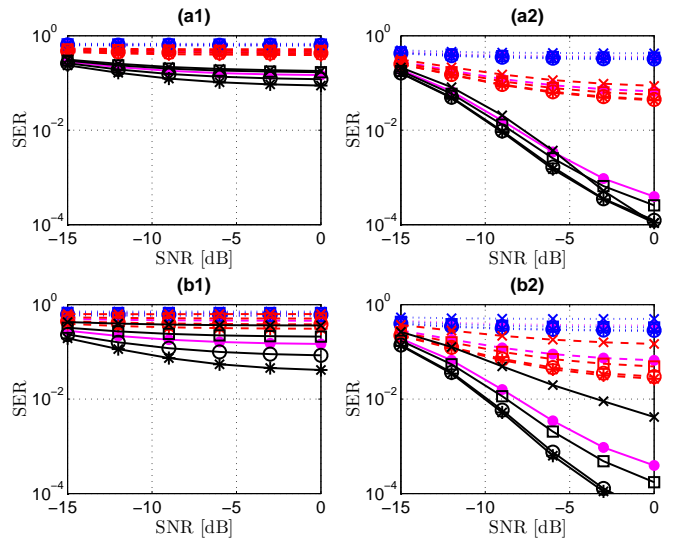


Figure 4: SER vs SNR (dB); SIR = -30 dB (continuous lines); SIR = -35 dB (dashed lines); SIR = -40 dB (dotted lines). DP: \bullet -marked curves; **Alg. 1**, $\gamma = 0$: $*$ -marked curves; **Alg. 1**, $\gamma = 2$: \circ -marked curves; **Alg. 1**, $\gamma = 2.3$: \square -marked curves; **min. LPI**: x -marked curves. **a1)** $\epsilon = 0.01$, MF; **a2)** $\epsilon = 0.01$, DF; **b1)** $\epsilon = 0.05$, MF; **b2)** $\epsilon = 0.05$, DF.

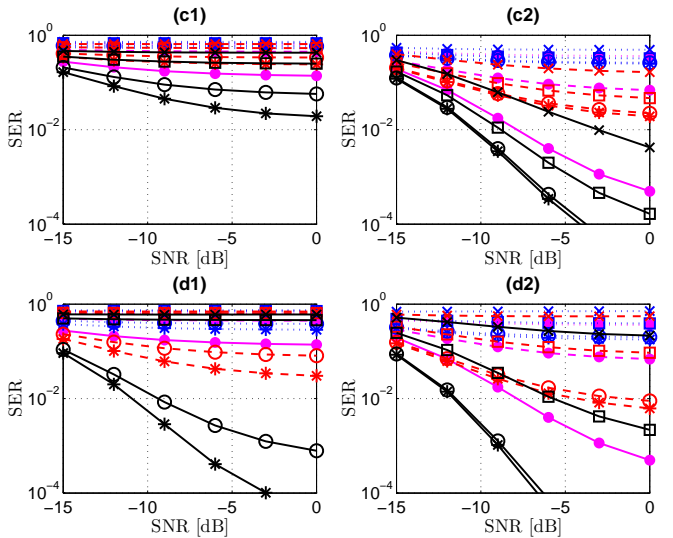


Figure 3: SER vs SNR (dB); SIR = -30 dB (continuous lines); SIR = -35 dB (dashed lines); SIR = -40 dB (dotted lines). WC: \bullet -marked curves; **Alg. 1**, $\gamma = 0$: $*$ -marked curves; **Alg. 1**, $\gamma = 2$: \circ -marked curves; **Alg. 1**, $\gamma = 2.3$: \square -marked curves; **min. LPI**: x -marked curves. **c1)** $\epsilon = 0.1$, MF; **c2)** $\epsilon = 0.1$, DF; **d1)** $\epsilon = 0.5$, MF; **d2)** $\epsilon = 0.5$, DF.

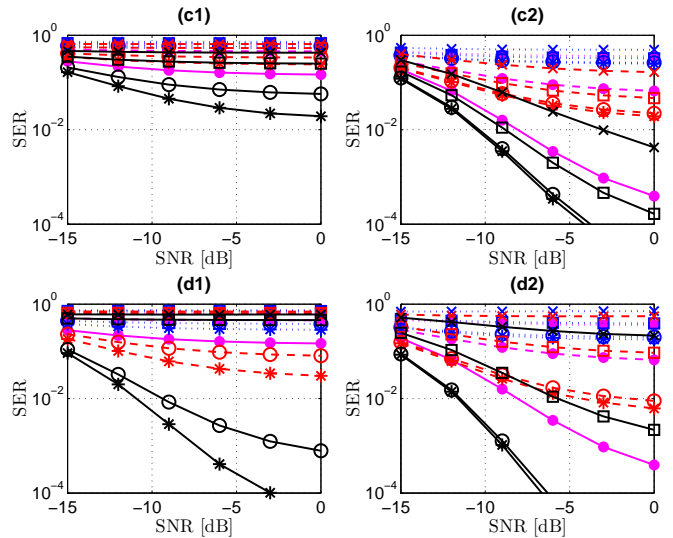


Figure 4: SER vs SNR (dB); SIR = -30 dB (continuous lines); SIR = -35 dB (dashed lines); SIR = -40 dB (dotted lines). DP: \bullet -marked curves; **Alg. 1**, $\gamma = 0$: $*$ -marked curves; **Alg. 1**, $\gamma = 2$: \circ -marked curves; **Alg. 1**, $\gamma = 2.3$: \square -marked curves; **min. LPI**: x -marked curves. **c1)** $\epsilon = 0.1$, DF; **c2)** $\epsilon = 0.1$, MF; **d1)** $\epsilon = 0.5$, MF; **d2)** $\epsilon = 0.5$, DF.

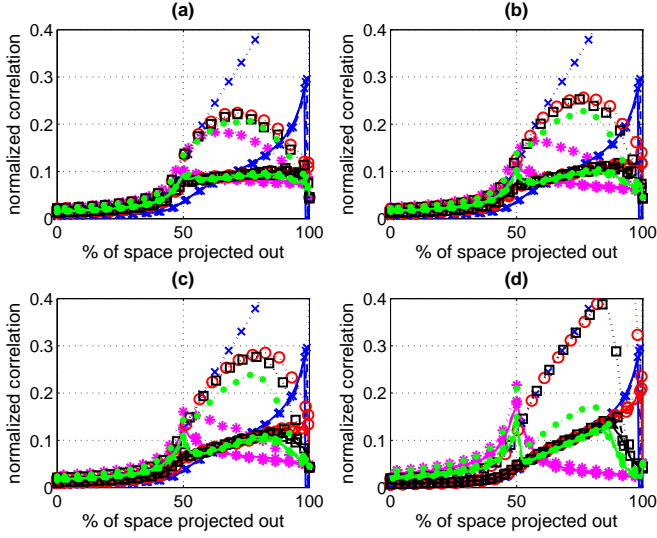


Figure 5: Intercept metric. Waveform 1 (dotted lines); waveform 2 (dashed lines); waveform 3 (dot-dashed lines); waveform 4 (continuous lines). EAW: x-marked blue curves; **Alg. 1**, $\gamma = 0$: o-marked red curves; **Alg. 1**, $\gamma = 2$: □-marked black curves; **Alg. 1**, $\gamma = 2.3$: ●-marked green curves; **min. LPI**: *-marked magenta curves. a) $\epsilon = 0.01$; b) $\epsilon = 0.05$; c) $\epsilon = 0.1$; d) $\epsilon = 0.5$.

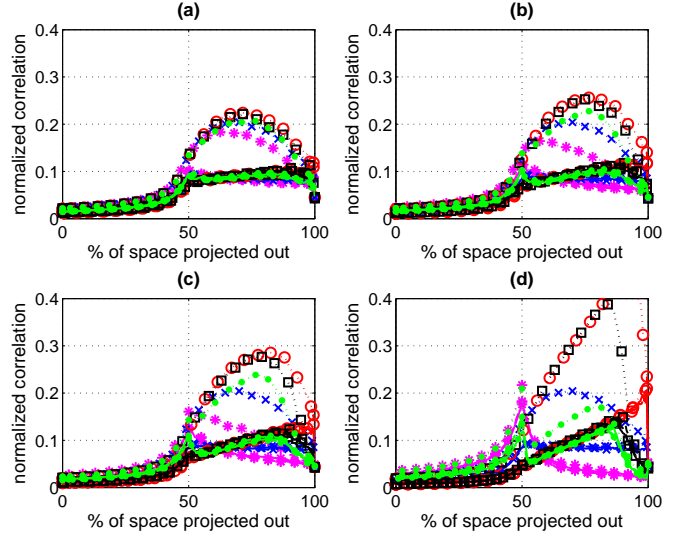


Figure 7: Intercept metric. Waveform 1 (dotted lines); waveform 2 (dashed lines); waveform 3 (dot-dashed lines); waveform 4 (continuous lines). DP: x-marked blue curves; **Alg. 1**, $\gamma = 0$: o-marked red curves; **Alg. 1**, $\gamma = 2$: □-marked black curves; **Alg. 1**, $\gamma = 2.3$: ●-marked green curves; **min. LPI**: *-marked magenta curves. a) $\epsilon = 0.01$; b) $\epsilon = 0.05$; c) $\epsilon = 0.1$; d) $\epsilon = 0.5$.

APPENDIX A EQUIVALENCE OF \mathcal{P}_4 AND \mathcal{P}_5

Let us assume that $[(z^*)^T \ y^*]^T$ is optimal to \mathcal{P}_5 ; then, it follows that $c^* = z^*/y^*$ is feasible to \mathcal{P}_4 , since:

$$\begin{aligned}
 & \text{tr} \left(Q_1 \begin{bmatrix} z^* \\ y^* \end{bmatrix} \begin{bmatrix} (z^*)^\dagger & (y^*)^* \end{bmatrix} \right) \geq 0 \\
 \Leftrightarrow & \text{tr} \left(\begin{bmatrix} -U_{k-1}^\dagger \widehat{W}^\dagger \widehat{W} U_{k-1} & U_{k-1}^\dagger \widehat{W}^\dagger \widehat{W} d_{0,k} \\ \left(U_{k-1}^\dagger \widehat{W}^\dagger \widehat{W} d_{0,k} \right)^\dagger & \epsilon - d_{0,k}^\dagger \widehat{W}^\dagger \widehat{W} d_{0,k} \end{bmatrix} \right. \\
 & \left. \begin{bmatrix} z^*(z^*)^\dagger & (y^*)^* z^* \\ y^*(z^*)^\dagger & |y^*|^2 \end{bmatrix} \right) \geq 0 \\
 \Leftrightarrow & (z^*)^\dagger (-U_{k-1}^\dagger \widehat{W}^\dagger \widehat{W} U_{k-1}) z^* + \\
 & 2\Re \left\{ (y^* U_{k-1}^\dagger \widehat{W}^\dagger \widehat{W} d_{0,k})^\dagger z^* \right\} + \\
 & |y^*|^2 (\epsilon - d_{0,k}^\dagger \widehat{W}^\dagger \widehat{W} d_{0,k}) \geq 0 \\
 \Leftrightarrow & (c^*)^\dagger (-U_{k-1}^\dagger \widehat{W}^\dagger \widehat{W} U_{k-1}) c^* + \\
 & 2\Re \left\{ (U_{k-1}^\dagger \widehat{W}^\dagger \widehat{W} d_{0,k})^\dagger c^* \right\} + \\
 & (\epsilon - d_{0,k}^\dagger \widehat{W}^\dagger \widehat{W} d_{0,k}) \geq 0 \tag{48}
 \end{aligned}$$

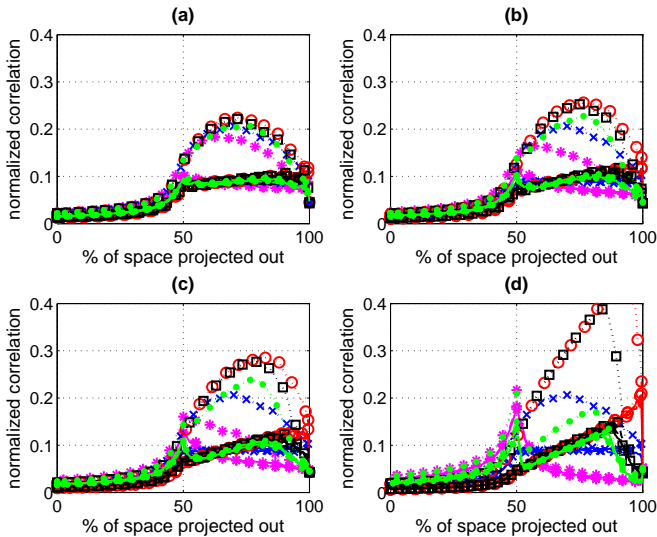


Figure 6: Intercept metric. Waveform 1 (dotted lines); waveform 2 (dashed lines); waveform 3 (dot-dashed lines); waveform 4 (continuous lines). WC: x-marked blue curves; **Alg. 1**, $\gamma = 0$: o-marked red curves; **Alg. 1**, $\gamma = 2$: □-marked black curves; **Alg. 1**, $\gamma = 3$: ●-marked green curves; **min. LPI**: *-marked magenta curves. a) $\epsilon = 0.01$; b) $\epsilon = 0.05$; c) $\epsilon = 0.1$; d) $\epsilon = 0.5$.

$$\begin{aligned}
 & \text{tr} \left(Q_2 \begin{bmatrix} z^* \\ y^* \end{bmatrix} \begin{bmatrix} (z^*)^\dagger & (y^*)^* \end{bmatrix} \right) = 1 \Leftrightarrow \\
 & \text{tr} \left(\begin{bmatrix} I & 0 \\ 0 & 0 \end{bmatrix} \begin{bmatrix} z^*(z^*)^\dagger & (y^*)^* z^* \\ y^*(z^*)^\dagger & |y^*|^2 \end{bmatrix} \right) = 1 \Leftrightarrow \\
 & \text{tr} \left((z^*)^\dagger z^* \right) = 1 = |y^*|^2 \Leftrightarrow (c^*)^\dagger c^* = 1. \tag{49}
 \end{aligned}$$

$$\begin{aligned} & \text{tr} \left(\mathbf{Q}_3 \begin{bmatrix} \mathbf{z}^* \\ \mathbf{y}^* \end{bmatrix} \begin{bmatrix} (\mathbf{z}^*)^\dagger & (\mathbf{y}^*)^* \end{bmatrix} \right) = 1 \Leftrightarrow \\ & \text{tr} \left(\begin{bmatrix} \mathbf{0} & \mathbf{0} \\ \mathbf{0} & 1 \end{bmatrix} \begin{bmatrix} \mathbf{z}^* (\mathbf{z}^*)^\dagger & (\mathbf{y}^*)^* \mathbf{z}^* \\ \mathbf{y}^* (\mathbf{z}^*)^\dagger & |\mathbf{y}^*|^2 \end{bmatrix} \right) = 1 \Leftrightarrow |\mathbf{y}^*|^2 = 1; \quad (50) \end{aligned}$$

Therefore, $v(\mathcal{P}_5) \leq v(\mathcal{P}_4)$. Conversely, if \mathbf{c}^* is the optimal to \mathcal{P}_4 , it can be shown that $[(\mathbf{c}^*)^T \mathbf{1}]^T$ is feasible to \mathcal{P}_5 . Indeed:

$$(\mathbf{c}^*)^\dagger \mathbf{c}^* = 1 \Leftrightarrow \text{tr} \left(\begin{bmatrix} \mathbf{I} & \mathbf{0} \\ \mathbf{0} & 0 \end{bmatrix} \begin{bmatrix} \mathbf{c}^* \\ 1 \end{bmatrix} \begin{bmatrix} (\mathbf{c}^*)^\dagger & 1 \end{bmatrix} \right) = 1; \quad (51)$$

$$\text{tr} \left(\begin{bmatrix} \mathbf{0} & \mathbf{0} \\ \mathbf{0} & 1 \end{bmatrix} \begin{bmatrix} \mathbf{c}^* \\ 1 \end{bmatrix} \begin{bmatrix} (\mathbf{c}^*)^\dagger & 1 \end{bmatrix} \right) = 1; \quad (52)$$

$$\begin{aligned} & (\mathbf{c}^*)^\dagger (-\mathbf{U}_{k-1}^\dagger \widehat{\mathbf{W}}^\dagger \widehat{\mathbf{W}} \mathbf{U}_{k-1}) \mathbf{c}^* + \\ & 2\Re \left\{ (\mathbf{U}_{k-1}^\dagger \widehat{\mathbf{W}}^\dagger \widehat{\mathbf{W}} \mathbf{d}_{0,k})^\dagger \mathbf{c}^* \right\} + (\epsilon - \mathbf{d}_{0,k}^\dagger \widehat{\mathbf{W}}^\dagger \widehat{\mathbf{W}} \mathbf{d}_{0,k}) \geq 0 \\ & \Leftrightarrow \text{tr} \left(\begin{bmatrix} -\mathbf{U}_{k-1}^\dagger \widehat{\mathbf{W}}^\dagger \widehat{\mathbf{W}} \mathbf{U}_{k-1} & \mathbf{U}_{k-1}^\dagger \widehat{\mathbf{W}}^\dagger \widehat{\mathbf{W}} \mathbf{d}_{0,k} \\ \left(\mathbf{U}_{k-1}^\dagger \widehat{\mathbf{W}}^\dagger \widehat{\mathbf{W}} \mathbf{d}_{0,k} \right)^\dagger & \epsilon - \mathbf{d}_{0,k}^\dagger \widehat{\mathbf{W}}^\dagger \widehat{\mathbf{W}} \mathbf{d}_{0,k} \end{bmatrix} \right. \\ & \left. \begin{bmatrix} \mathbf{c}^* (\mathbf{c}^*)^\dagger & \mathbf{c}^* \\ (\mathbf{c}^*)^\dagger & 1 \end{bmatrix} \right) \geq 0. \quad (53) \end{aligned}$$

Hence, $v(\mathcal{P}_4) \leq v(\mathcal{P}_5)$. Therefore, we can conclude that $v(\mathcal{P}_4) = v(\mathcal{P}_5)$.

REFERENCES

- [1] D. Ciuonzo, A. De Maio, G. Foglia, and M. Piezzo, "Pareto-theory for enabling covert intrapulse radar-embedded communications," in *Proc. of IEEE International Radar Conference*, Arlington (VA), US, May 2015.
- [2] S. D. Blunt, P. Yatham, and J. Stiles, "Intrapulse radar-embedded communications," *IEEE Trans. Aerosp. Electron. Syst.*, vol. 46, no. 3, pp. 1185–1200, Jul. 2010.
- [3] S. D. Blunt, J. G. Metcalf, C. R. Biggs, and E. Perrins, "Performance characteristics and metrics for intra-pulse radar-embedded communication," *IEEE J. Sel. Areas Commun.*, vol. 29, no. 10, pp. 2057–2066, Dec. 2011.
- [4] Z. Hijaz and V. S. Frost, "Exploiting OFDM systems for covert communication," in *IEEE Military Communications Conference (MILCOM)*, 2010, pp. 2149–2155.
- [5] D. Hounam and K.-H. Wagem, "A technique for the identification and localization of SAR targets using encoding transponders," *IEEE Trans. Geosci. Remote Sens.*, vol. 39, no. 1, pp. 3–7, Jan. 2001.
- [6] M. Onoe, N. Hasebe, and T. Zamas, "Radar reflectors with controllable reflection," *Electronics and Communications in Japan (Part I: Communications)*, vol. 63, no. 3, pp. 51–58, 1980.
- [7] B. H. Cantrell, J. O. Coleman, and G. V. Trunk, "Radar communications," Naval Research Lab Report, Tech. Rep. 8515, 1981.
- [8] D. M. Dobkin, *The RF in RFID: Passive UHF RFID in Practice*, ser. Communications engineering series. Elsevier Science, 2007.
- [9] H. Stockman, "Communication by means of reflected power," *Proceedings of the IRE*, vol. 36, no. 10, pp. 1196–1204, Oct. 1948.
- [10] D. L. Richardson, S. A. Stratmoen, G. A. Bendor, H. E. Lee, and M. J. Decker, "Tag communication protocol & system," Dec. 2001, US Patent 6,329,944.
- [11] R. M. Axline, G. R. Sloan, and R. E. Spalding, "Radar transponder apparatus and signal processing technique," Jan. 1996, US Patent 5,486,830.
- [12] D. Erricolo, H. Griffiths, L. Teng, M. C. Wicks, and L. L. Monte, "On the spectrum sharing between radar and communication systems," in *2014 International Conference on Electromagnetics in Advanced Applications (ICEAA)*, Aug. 2014, pp. 890–893.
- [13] D. W. Bliss, "Cooperative radar and communications signaling: The estimation and information theory odd couple," in *IEEE Radar Conference*, May 2014, pp. 50–55.
- [14] S. Boyd and L. Vandenberghe, *Convex Optimization*. New York, NY, USA: Cambridge University Press, 2004.
- [15] S. Sen, G. Tang, and A. Nehorai, "Multiobjective optimization of OFDM radar waveform for target detection," *IEEE Trans. Signal Process.*, vol. 59, no. 2, pp. 639–652, Feb. 2011.

- [16] A. De Maio, M. Piezzo, A. Farina, and M. Wicks, "Pareto-optimal radar waveform design," *IET, Radar, Sonar & Navigation*, vol. 5, no. 4, pp. 473–482, Apr. 2011.
- [17] W. Ai, Y. Huang, and S. Zhang, "New results on Hermitian matrix rank-one decomposition," *Mathematical Programming*, vol. 128, no. 1-2, pp. 253–283, 2011.
- [18] A. De Maio, Y. Huang, D. P. Palomar, S. Zhang, and A. Farina, "Fractional QCQP with applications in ML steering direction estimation for radar detection," *IEEE Trans. Signal Process.*, vol. 59, no. 1, pp. 172–185, Jan. 2011.
- [19] J. Capon, "High-resolution frequency-wavenumber spectrum analysis," *Proc. IEEE*, vol. 57, no. 8, pp. 1408–1418, Aug. 1969.
- [20] J. Li, J. R. Guerci, and L. Xu, "Signal waveform's optimal under restriction design for active sensing," in *4th IEEE Workshop on Sensor Array and Multichannel Processing*, 2006, pp. 382–386.
- [21] S. M. Kay, *Fundamentals of Statistical Signal Processing, Volume 2: Detection Theory*. Prentice Hall PTR, Jan. 1998.
- [22] B. Picinbono, "On deflection as a performance criterion in detection," *IEEE Trans. Aerosp. Electron. Syst.*, vol. 31, no. 3, pp. 1072–1081, 1995.
- [23] A. De Maio, M. Piezzo, A. Farina, and M. Wicks, "Pareto-optimal radar waveform design," in *International Waveform Diversity and Design Conference (WDD)*, 2010.
- [24] A. De Maio, M. Piezzo, S. Iommelli, and A. Farina, "Design of Pareto-optimal radar receive filter," *International Journal of Electronics and Telecommunications*, *JET*, vol. 57, no. 4, pp. 477–481, 2011.
- [25] A. Ben-Tal and A. S. Nemirovski, *Lectures on modern convex optimization: analysis, algorithms, and engineering applications*. Philadelphia, PA, USA: Society for Industrial and Applied Mathematics, 2001.
- [26] D. P. Palomar and Y. C. Eldar, *Convex optimization in signal processing and communications*. Cambridge University Press, 2010.

Domenico Ciuonzo (S'11-M'14) received the B.Sc. and M.Sc. (*summa cum laude*) degrees in computer engineering and the Ph.D., respectively in 2007, 2009 and 2013, from Second University of Naples (SUN), Aversa, Italy. In 2011 he was involved in the Visiting Researcher Programme of NATO CMRE, La Spezia, Italy. In 2012 he was a visiting scholar at the ECE Dept. of University of Connecticut (UConn), Storrs, US. In 2013-2014 he was a PostDoc at Dept. of Industrial and Information Engineering of SUN, under the project "MICENEA", funded by MIUR within the program Futuro in Ricerca (FIRB) 2013. Since 2014 he is a PostDoc researcher at DIETI, University of Naples, "Federico II", Italy. His research interests are mainly in the areas of Data Fusion, Statistical Signal Processing, Target Tracking and Wireless Sensor Networks. His reviewing activity was recognized by IEEE COMMUNICATIONS LETTERS and IEEE TRANSACTIONS ON COMMUNICATIONS, which nominated him "Exemplary Reviewer" in 2013 and 2015, respectively. Currently He serves as Associate Editor for the IEEE AEROSPACE AND ELECTRONIC SYSTEMS MAGAZINE.

Antonio De Maio was born in Sorrento, Italy, on June 20, 1974. He received the Dr.Eng. degree (with honors) and the Ph.D. degree in information engineering, both from the University of Naples Federico II, Naples, Italy, in 1998 and 2002, respectively. From October to December 2004, he was a Visiting Researcher with the U.S. Air Force Research Laboratory, Rome, NY. From November to December 2007, he was a Visiting Researcher with the Chinese University of Hong Kong, Hong Kong. Currently, he is an Associate Professor with the University of Naples Federico II. His research interest lies in the field of statistical signal processing, with emphasis on radar detection, optimization theory applied to radar signal processing, and multiple-access communications. Dr. De Maio is the recipient of the 2010 IEEE Fred Nathanson Memorial Award as the young (less than 40 years of age) AESR Radar Engineer 2010 whose performance is particularly noteworthy as evidenced by contributions to the radar art over a period of several years, with the following citation for "robust CFAR detection, knowledge-based radar signal processing, and waveform design and diversity".

Goffredo Foglia was born in Italy, in 1977. He received the Dr. Eng. Degree (Telecommunication Engineering) in June 2003 from the University of Naples Federico II, Italy, and the Ph.D. (Radar Theory and Techniques) in February 2007 from the University of Cassino. In February 2004 he joined Elettronica S.p.A., Rome, Italy. He is author of more than 30 papers on international journals and conferences. His research interest lies in the field of radar signal processing, electronic support measure algorithms, systems and jamming techniques.

Marco Piezzo received the Dr. Eng. degree (summa cum laude) in telecommunication engineering, and the Ph.D. degree in information engineering, both from the University of Naples Federico II, Italy, in 2009 and 2013, respectively. In the same university, he got a Postdoctoral Scholarship in the Department of Electrical Engineering and Information Technologies in 2013. In 2010 and 2012, he was a visiting student at the Chinese University of Hong Kong and the Hong Kong Baptist University, respectively. His research interest lied in optimization theory, with emphasis on radar signal processing. Currently, he is working at Elettronica S.p.A.